Channel Characterization and Wireless Communication Performance in Industrial Environments

JAVIER FERRER COLL

Doctoral Thesis in
Information and Communication Technology
Stockholm, Sweden 2014

TRITA ICT-COS-1402
ISSN 1653-6347
ISRN KTH/COS/R--14/02--SE

KTH Communication Systems
SE-100 44 Stockholm
Sweden

Akademisk avhandling som med tillstånd av Kungl Tekniska högskolan framlägges till offentlig granskning för avläggande av teknologie doktoralexamen i kommunikationssystem onsdagen den 4 juni 2014 klockan 13.00 i hörsal D i Forum, Kungliga Tekhniska Högskolan, Isafjordsgatan 39, Kista, Stockholm.

Tryck: Universitetsservice US AB

Abstract

The demand for wireless communication systems in industry has grown in recent years. Industrial wireless communications open up a number of new possibilities for highly flexible and efficient automation solutions. However, a good part of the industry refuses to deploy wireless solutions products due to the high reliability requirements in industrial communications that are not achieved by actual wireless systems. Industrial environments have particular characteristics that differ from typical indoor environments such as office or residential environments. The metallic structure and building dimensions result in time dispersion in the received signal. Moreover, electrical motors, vehicles and repair work are sources of electromagnetic interference (EMI) that have direct implications on the performance of wireless communication links. These degradations can reduce the reliability of communications, increasing the risk of material and personal incidents. Characterizing the sources of degradations in different industrial environments and improving the performance of wireless communication systems by implementing spatial diversity and EMI mitigation techniques are the main goals of this thesis work.

Industrial environments are generally considered to be environments with a significant number of metallic elements and EMI sources. However, with the penetration of wireless communication in industrial environments, we realize that not all industrial environments follow this rule of thumb. In fact, we find a wide range of industrial environments with diverse propagation characteristics and degradation sources. To improve the reliability of wireless communication systems in industrial environments, proper radio channel characterization is needed for each environment. This thesis explores a variety of industrial environments and attempts to characterize the sources of degradation by extracting representative channel parameters such as time dispersion, path loss and electromagnetic interference. The result of this characterization provides an industrial environment classification with respect to time dispersion and EMI levels, showing the diverse behavior of propagation channels in industry.

The performance of wireless systems in industrial environments can be improved by introducing diversity in the received signal. This can be accomplished by exploiting the spatial diversity offered when multiple antennas are employed at the transmitter with the possibility of using one or more antennas at the receiver. For maximum diversity gain, a proper separation between the different antennas is needed. However, this separation could be a limiting factor in industrial environments with confined spaces. This thesis investigates the implication of antenna separation on system performance and discusses the benefits of spatial diversity in industrial environments with high time dispersion conditions where multiple antennas with short antenna separations can be employed.

To ensure reliable wireless communication in industrial environments, all types of electromagnetic interference should be mitigated. The mitigation

of EMI requires interference detection and subsequent interference suppression. This thesis looks at impulsive noise detection and suppression techniques for orthogonal frequency division multiplexing (OFDM) based on wide-band communication systems in AWGN and multi-path fading channels. For this, a receiver structure with cooperative detection and suppression blocks is proposed. This thesis also investigates the performance of the proposed receiver structure for diverse statistical properties of the transmitted signal and electromagnetic interference.

Acknowledgements

First of all, I would like to thank my supervisors Dr. Slimane Ben Slimane and Dr. José Chilo. I feel fortunate to have these encouraging researchers who offered me important support during the past five years. I am also very grateful for the positive and fruitful discussions with Dr. Peter Stenumgaard who also has directed big part of my Ph.D. research.

This thesis is product of the "Reliable wireless machine-to-machine communications in the electromagnetic disturbed industrial environments" project founded by the Swedish Knowledge Foundation (KKS). Within this project, I would like to thank for the support provided from Stora Enso, SSAB, Green Cargo, Åkerströms, Syntronic, Agilent Technologies and FOI. Special thanks goes to the project colleagues at University of Gävle, Per Ängskog, Carl Elofsson and Carl Karlsson. Just thinking about the amazing time and experience gained during the multiple measurement campaigns, put a happy smile in my face.

I would like to thank my colleagues in the University of Gävle and in the Wireless department at KTH. Particularly, I would like to thank the present and former doctoral students, Sathyaveer Prasad, Per Landin, Charles Nader, Mohamed Hamid, Efrain Zenteno, Shoaib Amin, Indrawibawa Nyoman, Usman Haider, Mahmoud Alizadeh, Zain Ahmed Kahn, Rakesh Krishnan and Nauman Masud. I will never forget the incredible time and silly conversations during the fika time.

Finally, I would like to thank my family and friends; specially my parents, brother and sister for their motivation and encouragement during all these years of studies. The most important thanks goes to my half-orange Milena and my wonderful son Max for the incredible happiness that they bring to my life. They were supportive during the difficult moments and source of inspiration for my research.

Contents

List of Tables

List of Figures

List of Acronyms & Abbreviations

ADC	Analog-Digital Converter
APD	Amplitude Probability Distribution
AWGN	Additive White Gaussian Noise
BER	Bit Error Rate
CDF	Cumulative Distribution Function
CDMA	Code Division Multiple Access
CISPR	Comité International Spécial des Perturbations Radioélectriques
COST	European Cooperation in Science and Technology
dB	Decibel
dBm	Power relative to 1 milliwatt in dB
DECT	Digital Enhanced Cordless Telecommunications
EMC	Electromagnetic Compatibility
EMI	Electromagnetic Interference
GHz	Gigahertz
GUI	Graphical User Interface
IDFT	Inverse Discrete Fourier Transform
IEEE	Institute of Electrical and Electronics Engineers
IF	Intermediate Frequency
IPDP	In-Room Power Delay Profile
IR	Impulsive Rate

ISA	International Society of Automation
ISI	InterSymbol Interference
ISM	Industrial, Scientific and Medical radio bands
kHz	Kilohertz
KTH	Kungliga Tekniska Högskolan
LKAB	Luossavaara-Kiirunavaara Aktiebolag
LoS	Line of Sight
MHz	Megahertz
MIMO	Multiple-Input Multiple-Output
MLP	Multilayer Perceptron
MRC	Maximal Ratio Combining
MSE	Mean Square Error
M2M	Machine-to-Machine
NLoS	Non-Line of Sight
ns	Nano Seconds
OFDM	Orthogonal Frequency-Division Multiplexing
PAPR	Peak-to-Average Power Ratio
PC	Personal Computer
PDF	Probability Distribution Function
PDP	Power Delay Profile
PIFA	Planar-Inverted F Antenna
QAM	Quadrature Amplitude Modulation
RBW	Resolution Bandwidth
RF	Radio Frequency
rms	Root-Mean-Square
Rx	Receiver
SA	Signal Analyzer

SC	Selection Combining
SG	Signal Generator
SLM	Selected Mapping
SNR	Signal-to-Noise Ratio
SSAB	Swedish Steel Aktiebolag
Tx	Transmitter
VBW	Video Bandwidth
VNA	Vector Network Analyzer
WISA	Wireless Speaker and Audio
WLAN	Wireless Local Area Network
WSN	Wireless Sensor Network

Chapter 1

Introduction

1.1 Background

The demand for wireless communications has grown in recent years due to the increased use of mobile services. Broadband services demand high data rates to meet the requirements of mobile phones and industrial applications. The total mobile data traffic during the autumn of 2013 was 80% higher than that of 2012, and this trend is expected to continue in the coming years [1]. The industrial sector exhibits similar tendencies, and machine-to-machine (M2M) traffic is expected to increase 36-fold in 2018 relative to 2013 [2], as illustrated in Figure 1.1.

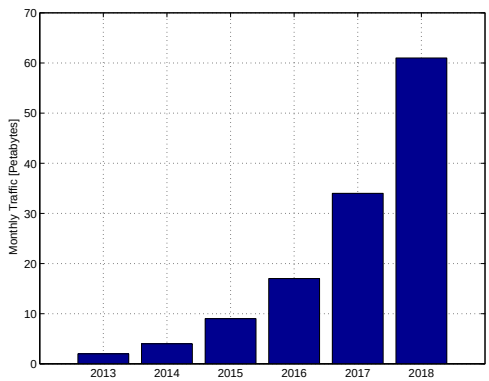

Figure 1.1: Forecast for machine-to-machine data traffic 2018.

The benefits that wireless applications bring to industry are growing due to the lower cost and flexibility of deploying new wireless communication systems. Moreover, the scalability and mobility of wireless systems open the door for improving the quality and

efficiency of industrial processes. However, the deployment of wireless solutions in industrial areas needs to overcome several requirements, such as levels of safety and reliability that are higher than those required by mobile services [3]. The particular characteristics of industrial environments tend to create different degradation sources that affect wireless communication. The metallic structure and large dimensions of buildings cause radio waves to reflect multiple times, creating a composition of transmitted signal replicas at the receiver. This fading effect can produce intersymbol interference (ISI) when the symbol period of the wireless system is shorter than the time dispersion of the channel [4]. Additionally, electromagnetic interference (EMI) generated by electric motors, power lines and maintenance activities contributes to the degradation of the received signal [5]. EMI has different statistical properties compared to additive white Gaussian noise (AWGN), thus systems designed to work in the presence of AWGN may not work properly in the presence of EMI.

Industrial environments have special propagation characteristics not present in typical office and residential environments. However, the majority of the indoor wireless systems designed to function in office environments are also used in industrial applications. Consequently, industrial wireless systems occasionally fail due to the EMI and high levels of time dispersion present in industrial environments. To provide reliable and robust communication, a number of improvements need to be elaborated upon. Thus, to improve current wireless systems, a radio channel characterization of multiple industrial environments, extracting the representative sources of degradation in each environment, should be performed.

Multiple wireless technologies are used in industrial applications, depending on the application requirements where the systems are deployed [6]. WLAN, WISA, WirelessHart, ZigBee, Bluetooth, DECT and ISA 100.11a are some of the most commonly used technologies in industrial areas. DECT is a mature technology that has been used since 1987 for cordless telephone service. WLAN technology works in the 2.4 GHz band and provides high data rates by using wide-band channels with orthogonal frequency division multiplexing (OFDM), which makes WLAN a perfect candidate for video streaming. WISA, WirelessHart, ISA 100.11a and ZigBee have been developed to manage a large number of devices in a network with low data rates and are suitable for wireless sensor network (WSN) services. Currently, all of these technologies are widely deployed in industrial environments [7], but they require constant development and new versions to address the challenges and needs of industrial applications. For instance, Figure 1.2 shows the performance of different standards when an interference source is present in the environment. High data rates can be achieved when implementing wide-band communication systems, such as WLAN systems; however, the communication delay can reach hundreds of milliseconds, risking the reliability of some industrial processes.

A number of studies have characterized typical industrial environments with large dimensions and metallic structures, showing high time dispersion levels [8, 9]. However, few studies have investigated the time dispersion of industrial environments with different structural characteristics. Moreover, distance path loss characterization studies performed by various research groups in multiple industrial environments have found path loss exponents lower than the corresponding free space exponent, i.e., $\alpha = 2$ [9, 10]. However, the

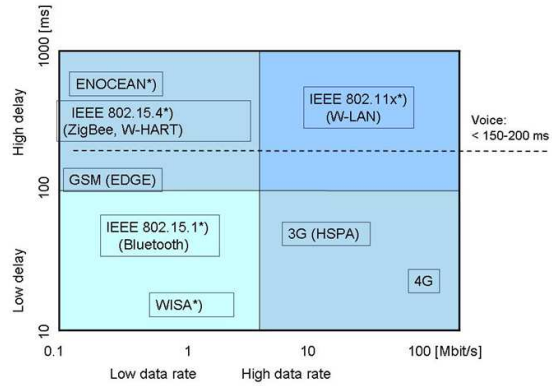

Figure 1.2: A comparison of wireless standards in terms of data rate and time delay under an interference source.

estimation of the frequency path loss in a wide frequency band in industrial environments has not been explored in many studies. Additionally, previous studies have analyzed EMI in industrial environments by exploring low-frequency bands [11, 12]. However, little research has been conducted over a wide range of frequencies, i.e., up to 3 GHz, where a number of industrial wireless systems operate. Thus, a significant effort must be undertaken to characterize and understand the degradations found in wireless systems deployed in industrial environments.

To reduce the impact of time dispersion, path loss and EMI in wireless communications, a number of techniques can be implemented. In this thesis, spatial diversity and EMI mitigation techniques in OFDM systems are investigated to improve the performance of wireless system in industrial environments.

Antenna diversity can be one solution to mitigate amplitude fade at certain locations [13, 14]. Using two or more antennas separated by a certain distance at the transmitter or receiver and combining the received signals can increase the signal quality and the overall system performance. Some industrial processes require high reliability levels, i.e., good signal quality, and spatial diversity can be used to fulfil this requirement. However, the physical limitations inherent at certain locations do not permit the use of wide antenna separations. Little research has been performed to investigate the potential benefits of using spatial diversity with short antenna separations in industrial environments [15].

Furthermore, the EMI degradation found in industrial environments can be mitigated by detecting and suppressing this interference. Previous studies have developed techniques to detect impulsive noise in OFDM systems [16, 17]. However, their efficiency depends on the statistical properties of the transmitted signal and the impulsive noise. Regarding the suppression of the impulsive noise, previous studies have investigated the mitigation of impulsive noise by non-linear clipping and blanking methods [18, 19] and by using a pre-

demodulated estimation of the OFDM signal [20]. However, the efficiency of these suppression techniques is dependent on the impulse noise detection and the statistical properties of the transmitted signal. Thus, a receiver structure composed of cooperative detection and suppression needs to be investigated.

1.2 Problem Formulation

The wide-scale deployment of wireless communications systems in industrial environments is a long process that needs to overcome multiple challenges. Reliable communication is one of the most important challenges that have to be solved in order to increase the confidence of the industrial sector for deploying wireless solutions. Industrial wireless applications demand reliable and robust communication systems due to the potential risks associated with some applications. The industry encompasses a wide range of environments with different channel characteristics and thus different sources of degradation, risking the system's reliability.

Understanding the characteristics of the communication channel is necessary for designing a good communication system. Industrial environments typically have significant time dispersion due to the metallic structures and large dimensions of obstacles. They are commonly characterized in the literature as multi-path fading channels with long time delay spread. However, as the penetration of wireless communication systems in industrial applications increases, we see an increased diversity in industrial environments with a wide range of structural properties. This means that one has to be careful when designing a good communication system for industrial environments since a channel model obtained from one industrial environment may be not suitable for another industrial environment. The path loss in industrial environments can also be quite different from that in commercial non-industrial environments. Non line-of-sight (NLoS) situations can cause coverage problems at certain frequency bands. EMI generated by electrical motors, repair work, and transportation systems is another source of interference that affects the performance of wireless system in industrial environments. Hence, wireless system developers have to take the presence of such interference into account in their design process to ensure reliable communications in industrial environments.

Few measurement campaigns have explored the radio channel characteristics in different industrial environments. However, assuming that industrial environments present similar propagation conditions and interference could result in the design of unreliable communication systems. Our first objective in this thesis work is to investigate the implications of the diverse structural properties of industrial environments on the characteristics of radio communication channels.

Improving the performance of wireless communication systems in multi-path fading channels is achieved by the use of diversity techniques, where the receiver receives multiple replicas of the same signal transmitted through independent fading multi-path channels. Diversity can improve both the received signal strength and the time availability of the signal at the receiver. Spatial diversity is the most efficient diversity method in wireless communications. It can improve the performance of wireless links without any loss of effi-

ciency. However, the diversity gain from using spatial diversity depends on the separation between the receiver antennas. For multi-path fading channels with diffused multi-path components only, a separation of $\lambda/2$ is usually enough to ensure a maximum diversity gain. However, in some industrial environments, it may not be possible to ensure a separation of $\lambda/2$. Having an antenna separation above $\lambda/2$ may not provide the necessary diversity gain for reliable communication in industrial environments. Therefore, the second objective in this thesis work is to investigate the effect of antenna separation on the diversity gain in wireless communication links in industrial environments.

Diversity techniques may not be able to provide the expected performance in the presence of additive electromagnetic interference. Hence, to ensure reliable communications in industrial environments, this type of impulsive noise needs to be mitigated from the received signal before signal detection. The mitigation of the impulsive noise usually includes interference detection followed by interference suppression stages. The existing interference detection techniques provide good performance at certain impulsive rates and for Gaussian type transmitted communication signals. Hence, their efficiency is linked to the statistical properties of the impulsive noise source and that of the transmitted communication signal. The performance of the impulsive noise suppression is dependent on the impulsive samples detected in the received signal. Thus, by increasing the detected impulsive noise samples, additional impulsive noise can be suppressed from the received signal, leading to a better performance of the wireless communication link in industrial environments. Our third objective in this work is to investigate the effects of impulsive noise detection and suppression techniques on the performance of wireless communication links in AWGN and multi-path fading channels. We further propose an efficient receiver structure for the transmitted signal and impulsive noise with different statistical properties.

1.3 Thesis Outline and Contributions

The main contributions of the thesis are based on a characterization of the radio channel for different industrial environments, performing measurements and introducing techniques for improving the performance of industrial wireless systems. We next give an outline of the thesis and describe the contributions within each chapter.

Chapter 2 describes the industrial environments characterized during the measurement campaigns performed in this thesis and the measurement setups used during this characterization . The chapter details a wide variety of industrial environments with diverse propagation characteristics, such as a bark furnace, metal works, paper warehouse, outdoor industrial environment, laboratory and office, rail yard and a mine tunnel. The environments described in this chapter are referred to throughout the thesis, providing a guide of the characterized industrial environments. The measurement setups presented in the chapter are also referred to in the remaining chapters.

Chapter 3 presents the multi-path characterization performed in industrial environments with diverse propagation characteristics. The chapter contains a characterization from environments with large amounts of metallic objects, i.e., a bark furnace, to environments with special characteristics that reduce multi-path propagation, i.e., a paper

warehouse. The chapter shows the diverse behavior of the multi-path propagation in industry in contrast to previous studies reported in the literature. This chapter is based on the investigations performed in Papers [J1], [J2], [J3], [J4], [C2], [C3] and [C4].

Chapter 4 addresses radio-wave propagation path loss in industrial environments. The chapter provides measurements and models of the frequency dependence of the received signal strength in NLoS scenarios. The obtained results show that the frequency dependence is more pronounced in NLoS scenarios with radio-wave absorbing properties relative to environments with high multi-path propagation. The content of this chapter is manly based on the measurement results presented in Paper [J3].

Chapter 5 presents an EMI characterization for a broad frequency band in multiple industrial environments. Various sources of EMI such as electrical motors, vehicles and repair work are analyzed during the measurement campaigns. A number of these EMI sources in industrial environments are found to have higher frequency components than those reported earlier in the literature. The measured EMI in the bark furnace is modeled statistically and used to investigate the effect of such EMI on the performance of the wireless systems. This chapter is based on the measured interferences at various industrial locations presented in Papers [J1], [J2], [J4] and [C1].

Chapter 6 studies the benefits of implementing spatial diversity in industrial environments with high multi-path propagation conditions. In particular, this chapter investigates the spatial diversity gain achieved using short antenna separations. Substantial benefits to the system performance can be obtained by applying diversity techniques with short antenna separations in industrial environments having high multi-path propagation. This study is based on the measurement results reported in Paper [J5].

Chapter 7 proposes a receiver structure for OFDM-based systems for industrial environments. The receiver is a combination of impulsive noise detection and suppression stages, providing robustness against fading multi-path channels and EMI. The chapter also discusses the implication of the statistical properties of the transmitted signal and impulsive noise on the detection and suppression. This chapter is based on the results presented in Papers [J6] and [C5].

Chapter 8 concludes the contributions of the thesis work and suggests a number of directions for future research.

1.4 Publications

This doctoral thesis is the product of research studies submitted or accepted in international conferences and journals. The following list presents the peer review articles included in this thesis:

[J.1] J. Ferrer-Coll, P. Ängskog, J. Chilo and P. Stenumgaard, “Characterization of electromagnetic properties in iron-mine production tunnels,” *IET Electronics Letters,* vol.48, no.2, pp.62-63, Jan. 2012.

[J.2] J. Ferrer Coll, J. Chilo and S. Ben Slimane, "Radio-frequency electromagnetic characterization in factory infrastructures," *IEEE Trans. on Electromagnetic Compatibility,* vol.54, no.3, pp.708-711, Jun. 2012.

[J.3] J. Ferrer-Coll, P. Ängskog, J. Chilo and P. Stenumgaard, "Characterization of highly absorbent and highly reflective radio wave propagation environments in industrial applications," *IET Communications,* vol.6, no.15, pp.2404-2412, Oct. 2012.

[J.4] P. Stenumgaard, J. Chilo, J. Ferrer-Coll and P. Ängskog, "Challenges and conditions for wireless machine-to-machine communications in industrial environments," *IEEE Communications Magazine,* vol.51, no.6, pp.187-192, Jun. 2013.

[J.5] J. Ferrer-Coll, P. Ängskog, C. Elofsson, J. Chilo and P. Stenumgaard, "Antenna cross correlation and ricean K-factor measurements in indoor industrial environments at 433 MHz and 868 MHz," *Wireless Personal Communications,* vol.73, no.3, pp.587-593, May. 2013.

[J.6] J. Ferrer-Coll, B. Slimane, J. Chilo and P. Stenumgaard, "Detection and Suppression of Impulsive Noise in OFDM Receiver," *Wireless Personal Communications,* Submitted Feb. 2014.

[C.1] P. Ängskog, C. Karlsson, J. Ferrer Coll, J. Chilo and P. Stenumgaard, "Sources of disturbances on wireless communication in industrial and factory environments," in *Asia-Pacific International Symposium on Electromagnetic Compatibility,* Beijing, Apr. 2010, pp. 285-288.

[C.2] J. Ferrer Coll, P. Ängskog, C. Karlsson, J. Chilo and P. Stenumgaard, "Simulation and measurement of electromagnetic radiation absorption in a finished-product warehouse," in *IEEE International Symposium on Electromagnetic Compatibility,* Fort Lauderdale-Florida, vol.3, Jul. 2010, pp. 881-884.

[C.3] J. Ferrer-Coll, J. Dolz Martin de Ojeda, P. Stenumgaard, S. Marzal Romeu and J. Chilo, "Industrial indoor environment characterization - Propagation models," in *IEEE Electromagnetic Compatibility Symposium in Europe,* York, Sep. 2011, pp.245-249.

[C.4] J. Ferrer Coll, P. Ängskog, H. Shabai, J. Chilo and P. Stenumgaard, "Analysis of wireless communications in underground tunnels for industrial use," in *IEEE International Conference in Industrial Electronics IECON,* Montreal, Oct. 2012, pp.3216-3220.

[C.5] J. Ferrer-Coll, B. Slimane, J. Chilo and P. Stenumgaard, "Impulsive Noise Detection in OFDM Systems with PAPR Reduction," accepted for publication in *IEEE Electromagnetic Compatibility Symposium in Europe,* Gothenburg, Sep. 2014.

Chapter 2

Industrial Environments

2.1 Introduction

Industrial environments have generally been considered environments with large dimensions and numerous metallic elements that increase multi-path propagation as well as with diverse electric machinery, transportation equipment and repair work that contribute to EMI [11, 21–23]. This general description of an industrial environment is valid for a certain percentage of industrial environments. However, the measurement campaigns carried out during this thesis work showed that industrial environments are not always highly reflective containing EMI. In fact, a number of industrial environments do not follow this general description, presenting particular characteristics that in some cases result in the opposite propagation behavior. In this thesis work, we attempt to present a number of diverse industrial environments with the objective of covering a wide range of industrial environments.

This chapter describes the various industrial environments where the measurement campaigns were performed. Four industrial companies located in Sweden cooperated with this study; Stora Enso, Swedish Steel Aktiebolag (SSAB), Green Cargo and Luossavaara-Kiirunavaara Aktiebolag (LKAB). Stora Enso is a paper manufacturer that processes trees into final products, e.g., biomaterial, wood or paper. SSAB is a steel works company that processes raw minerals into steel. Green Cargo is a logistics company that uses trains as their main transportation system. LKAB is a mining company that extracts iron-ore from their mines. By exploring multiple diverse industrial environments, we attempt to show the significant diversity of industrial scenarios. From typical industrial environments following the general description presented above to environments with different characteristics and opposite behavior. The different environments described in this chapter are investigated in the following chapters; therefore, this chapter is referred to throughout the thesis.

The next section of this chapter presents the descriptions of six distinct industrial environments as well as laboratory and corridor environments. The third section contains the measurement setups used during the environment characterization. The last section provides a summary of the chapter.

2.2 Environment Descriptions

Industrial environment is a term used to describe environments under harsher conditions than typical office environments. The different conditions that can be found in industry can degrade the performance of wireless systems. Depending on the characteristics of the environment, such as dimensions, materials and the presence of electronic equipment, the propagation channel will be subject to different types of degradations. In this section, we describe a wide range of industrial environments, from typical industrial environments with large dimensions and metallic surfaces to environments with special characteristics such as a paper warehouse and a mine tunnel.

2.2.1 Bark Furnace

The bark furnace is a highly reflective environment, where the ceiling and walls are metallic, and the floor is asphalt. The bark furnace contains large amounts of metallic objects and machinery. This type of environment corresponds to the scenario where we could expect to find high levels of multi-path fading. The metallic structures increase the reflection of signals and create a received signal with numerous multi-path components with long delays. For instance, the scenarios shown in Figure 2.1 correspond to indoor locations for burning wood waste at the paper mill in Stora Enso, Borlänge. This building has nine floors with a total height of 30 m and a partially free sight between floors. The walls and ceiling are metallic, and there is a high density of metallic machinery, pipes and columns. DECT and WLAN systems are deployed in this facility for machine-to-machine communication and for worker communication.

Figure 2.1: Reference locations for bark furnace at the paper mill.

2.2.2 Metal Works

Metal works are usually buildings with large dimensions and metallic objects present. This typical environment can be found in a large percentage of the industry. Photographs of two factory halls are shown in Figure 2.2, a production hall in a steel works and a finished steel

product warehouse at SSAB in Luleå and Borlänge, respectively. In the production hall in the steel works, the floor is made of asphalt, the walls contain metallic materials, the building has dimensions of 25.5 m x 150 m x 12.5 m and large cranes hang from the metallic ceiling. The general difference between this environment and the previous environment, i.e., the bark furnace or highly reflective environment, is that the previous environment has smaller dimensions and a much higher density of metallic objects, often producing NLoS situations. Many wireless systems working in different industrial, scientific and medical (ISM) bands, such as WLAN, DECT, Bluetooth, ZigBee and Åkerströms Remotus, can be found in this type of environment.

Figure 2.2: Large industrial halls at metal works.

2.2.3 Paper Warehouse

This environment corresponds to a warehouse containing paper rolls at the Stora Enso paper mill in Borlänge. The environment consists of a warehouse where the final products, i.e., paper rolls, are stacked in blocks that are separated by corridors. As shown in Figure 2.3, the environment where the storage plan covers an area of 85 m x 150 m and has a ceiling height of 8 m. The walls and ceilings are constructed of prefabricated concrete, and the floor is made of concrete. The paper rolls have a diameter between 1.25 m and 1.70 m, a height between 1 m and 3 m and weights between 300 kg to 1200 kg. This paper exhibits special dielectric properties, causing the absorption of the incident signals in the paper rolls. This environment is quite unique; the channel propagation behaves in a manner opposite of the typical industrial environments with high multi-path levels. WLAN system and Åkerströms Sesam utilizing the 869.8 MHz frequency band for door openers are present in this environment.

2.2.4 Outdoor Industrial Environment

Outdoor industrial environments are often used for the purposes of transporting and storing goods. A process in the steel works at SSAB in Luleå is shown in Figure 2.4 (left), where the coal is heated in ovens to increase the purity and efficiency of the coal for later use.

Figure 2.3: Corridor of paper rolls at the warehouse.

Figure 2.4 (right) shows a storage area where a crane lifts trees from the incoming trucks and places them in piles. Outdoor environments usually have few reflective surfaces and thus should not exhibit high levels of multi-path. However, transportation and electric machinery can be a potential source of EMI. WLAN and Bluetooth systems are present in this environment.

Figure 2.4: Outdoor scenarios in the steel works factory and paper mill.

2.2.5 Laboratory and Office

A laboratory and office environment are described in this section. These environments are used to test the measurement setups and to evaluate their performance. The first scenario is a radio frequency (RF) laboratory for testing microwave equipment, such as RF amplifiers, antennas and analog-digital converters (ADC), at the University of Gävle. The environment has electronic instruments stacked in racks and tables containing electronic components and computers. The laboratory room has dimensions of 9.5 m x 6.5 m x 3 m. The floor, walls and ceiling are made of concrete, and the windows have high RF isolation between outdoor and indoor signals. A photograph of the laboratory is shown in Figure 2.5 (left).

The second scenario consists of a long corridor with laboratory rooms on one side and office rooms on the other side. The floor, ceiling and wall on the laboratory side are made of concrete, and the office side is made of glass walls and wooden doors. The corridor is 84 m x 1.8 m x 3 m. Figure 2.5 (right) shows the corridor with the multi-path measurement setup. A WLAN system is used in this environment.

Figure 2.5: RF laboratory and office corridor environments.

2.2.6 Rail Yard

Rail yards are environments that have large dimensions containing multiple rail tracks and electric pantographs. Marshalling yards were scanned to find EMI at the Green Cargo facilities in Borlänge, Göteborg, Luleå and Stockholm. Figure 2.6 illustrates a train engine (left) and a marshalling yard where the measurements were performed (right). Åkerströms Locomote wireless system in the 410 - 480 MHz frequency band is used to control the locomotives in the rail yard.

Figure 2.6: Train engine in Borlänge and rail yard in Stockholm area.

2.2.7 Mine Tunnel

Mine tunnels are environments with rail tracks that are used to transport minerals inside the mine. The mine tunnel measurements were performed in the iron-ore mine at LKAB in Kiruna and in a tunnel located at SSAB in Oxelösund. The mine has different underground levels, and in this case, the measurements were performed in a level 1045 m below the top of the mountain. In this level, two locations are analyze: one in a narrow tunnel with a single rail track and another in a joint point where the narrow tunnel joins a wide tunnel with two tracks. The narrow tunnel is 4.2 m wide and has a height of 4.6 m, and the wide tunnel is 7.1 m wide and has a height of 6.1 m high. Figure 2.7 shows the two locations where the measurements were carried out in the mine tunnel. WLAN and Åkerströms Locomote systems are present in this environment.

Figure 2.7: Wide tunnel and joint point in the iron-ore mine.

2.3 Measurement Setups

The environments described in this chapter are characterized and used to test the improvements proposed in this thesis. To perform the measurements, different measurement setups were used. This section presents two measurement setups used to characterize the environments and test the improvements. The first is based on performing the measurements in a vector network analyzer (VNA) and the second by using a spectrum analyzer (SA).

2.3.1 Network Analyzer Setup

This measurement setup was developed to quantify the time dispersion or multi-path in the different industrial environments. The setup shown in Figure 2.8 is composed of a vector network analyzer, an ultra-wide-band omnidirectional antenna pair connected to the analyzer by low-attenuation coaxial cables, and a computer with a graphical user interface (GUI) that controls the entire system. The setup is calibrated for each frequency band measured. This measurement setup was used to obtain the frequency response of the channel and subsequently compute the channel impulsive response.

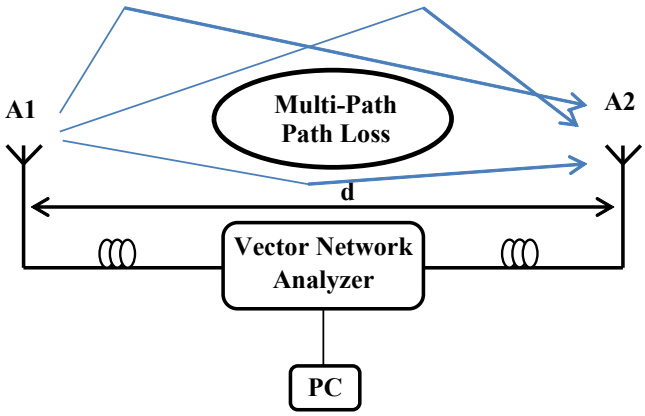

Figure 2.8: Network analyzer measurement setup.

To perform the channel characterization measurements with the VNA, several parameters need to be adjusted. For instance, the system has a maximum detectable delay, τ_{max}, after which the multi-path components are not captured. The maximum detectable delay is obtained as follows

$$\tau_{\max} = \frac{N_{\text{points}} - 1}{BW} \tag{2.1}$$

where N_{points} is the number of measurement points used in one sweep and BW is the bandwidth selected. The system uses 1601 points and 500 MHz of bandwidth, providing a maximum detectable delay of 3.2 μs, which is sufficient to cover most indoor environments. Consequently, the time resolution for distinguishing two consecutive paths in this case is 2 ns.

Another parameter that should be taken into account is the frequency shift, Δf, which is a function of the propagation time, t_{tr} (time of flight), the frequency span, S, and the sweep time, t_{sw}, as defined by the following expression

$$\Delta f = t_{tr}\,(S/t_{sw}) \tag{2.2}$$

The intermediate frequency (IF) bandwidth should be greater than Δf. With a frequency span of 500 MHz S, a sweep time of 800 ms, and not expecting to detect multi-path components after 2 μ s, we require an IF bandwidth greater than 1.25 kHz.

2.3.2 Generic Spectrum Analyzer Setup

This generic spectrum analyzer setup is used to measure the path loss and EMI present in the environments as well as to test the spatial diversity and EMI mitigation techniques. The

setup shown in Figure 2.9 is based on stimulating the channel with a signal generator (SG) and measuring the response of the channel with a spectrum analyzer.

Depending on the parameter measured, this generic setup is adjusted to the respective requirements. For instance, the EMI measurement setup is composed of a broadband antenna and a spectrum analyzer that measures the EMI source. In the case of the path loss measurements, the setup uses an SG to excite the channel and two antennas connected to the SA to capture the combined signal. The measurement setup used for the spatial diversity test is similar to the path loss setup; however, the received signals by the two antennas are captured in two SAs processing them independently. The EMI mitigation measurement setup is composed of an SG and an SA, forming a communication system, and an interference source produced by a second SG.

The center frequency, bandwidth, resolution bandwidths, distance between antennas and other settings and steps performed during each measurement are described in the following chapters.

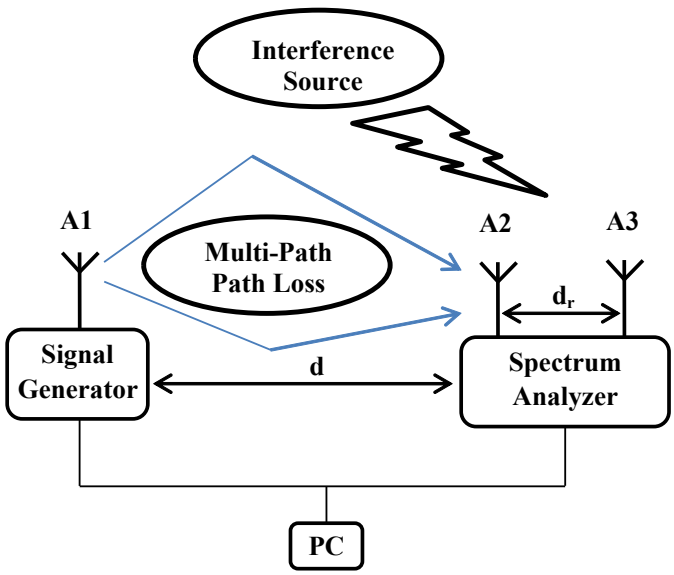

Figure 2.9: Generic spectrum analyzer measurement setup.

2.4 Summary

This chapter presented a broad variety of industrial environments and the measurement setups used during the environment characterization. With our selection of these different environments, we have attempted to cover a large percentage of the environments encountered in industry. From typical industrial environments, with large amounts of metallic ob-

jects exhibiting a highly reflective propagation, to mine tunnels or paper warehouse, with opposite characteristics and behavior. This does not mean that we have covered all possible industrial environments, but we believe that the selected environments will illustrate the differences in radiowave propagation when going from one environment to another. The industrial environments and the measurement setups described in this chapter will be referred to regularly in the following chapters.

Chapter 3

Multi-path Characterization in Industrial Environments

3.1 Introduction

Multi-path fading is an effect produced when a signal propagates through a dispersive channel. This time dispersion is a consequence of the multiple replicas of the signal that are produced by reflection, diffraction and scattering with the objects encountered in the channel arriving at the receiver. The number of replicas in the received signal depends on the nature of the objects encountered in the environment. Thus, an industrial environment with metallic surfaces will introduce high levels of multi-path fading compared to other indoor environments such as office or residential environments. High levels of multi-path could produce intersymbol interference (ISI), reducing the communication performance. The reduction in communication performance depends on the duration of the symbol period of a radio system and the dispersive properties of the environment [24]. Multiple-input and multiple-output (MIMO) can take advantage of the high levels of multi-path. High levels of multi-path produce uncorrelated signals in each antenna, and by combining the received signals in a special manner, MIMO systems can increase the performance of the system. Thus, environments with low multi-path levels will not experience ISI, and deploying MIMO systems in these environments will not increase the communication performance. Consequently, there is a need for understanding the channel behavior when deploying a new wireless system. Selecting an adequate system for each scenario will increase the reliability of communications.

A number of studies have characterized and modeled the dispersive properties of the channel, quantifying its dispersion with the root-mean-square (rms) delay spread. For instance, the research performed in [25] contains a channel characterization in office environments in the wide-band between 2 and 5 GHz. This paper shows rms delay spread values ranging from 30 ns in line-of-sight (LoS) situations to 50 ns in non line-of-sight (NLoS) situations. An extensive measurement campaign in residential and commercial areas performed by Ghassemzadeh *et al.* [26] found rms delay spread levels of 3.38 ns

in LoS and 8.15 ns in NLoS, and they also proposed a propagation model to match the measurement results.

Measurements carried out in industrial environments with a significant number of metallic surfaces showed that the rms delay spread has levels of approximately 50 ns [21]. In that study, the authors proposed a modification of the Saleh-Valenzuela indoor model that provides a better approximation to their measurement results. The researchers in [9] performed measurements in a nuclear power plant and in a chemical pulp factory, concluding that these environments exhibit significant time dispersion and thus provide good received signals in non-line-of-sight scenarios. A study of signal fading due to obstructed paths and multi-path in industrial environments in the 1.8 and 2.4 GHz ISM bands was presented in [22]. A measurement in a subway tunnel in the 2.4 GHz band reported high rms delay spread levels from 159 ns in LoS to 234 ns in NLoS scenarios [27]. In contrast, several measurement studies performed in tunnel mines found low levels of rms delay spread [28, 29].

Based on the overall picture of the measurement results in the literature, industrial environments are considered reflective due to the quantities of metallic objects present in such environments. This chapter shows that generalizing all industrial environments as reflective does not correspond to reality. This thesis develops a measurement setup for characterizing industrial environments with completely different characteristics as discussed in Chapter 2. The work of this chapter is based on published articles. In Papers [J2] and [J4], typical reflective industrial environments with a significant number of metallic objects and high rms delay spread are studied. An industrial environment with a lower rms delay spread relative to office environments due to the absorbing materials stored in the hall is analyzed in Paper [C2]. Moreover, tunnel environments with low multi-path components are presented in Papers [J1] and [C4]. To complete this channel characterization, the Saleh-Valenzuela and in-room power delay profile (IPDP) propagation models that extract the model parameters for the different industrial environments are presented in Papers [C3] and [J3].

The remainder of this chapter is structured as follows. The next section presents the theoretical background necessary to understand the extracted channel characteristics. The third section presents the results of the measurement campaigns in the different environments and the corresponding multi-path parameters that quantify the time dispersion in the environment such as the rms delay spread. This third section also contains the Saleh-Valenzuela and IPDP extracted parameters models of the different environments. The last section provides a summary of the chapter with general conclusions.

3.2 Multi-path Fading in Wireless Communications

The impulse response describes the time dispersive properties of a channel and can be used to characterize an environment. Obtaining the frequency response of the channel in a certain band can be used to estimate the impulse response of the channel. In our work, the frequency response was determined by performing a spectral analysis of the channel with a vector network analyzer (VNA), which obtains the complex channel transfer function, $H_m(f)$. Once the transfer function is in the PC, it is weighted through a Blackman-Harris

window in order to reduce the out-of-band noise [30]. Assuming that the channel is time invariant compared with the transmitted signal, i.e., the channel variations are slower than the base-band signal variations, then the channel transfer function after windowing can be written as follows

$$H_c(f) = H_w(f) \times H_m(f) \tag{3.1}$$

Hence, the impulse response of the radio channel is obtained by taking the inverse Fourier transform approximated by using the inverse discrete Fourier transform (IDFT)

$$\begin{aligned} h_c(\tau) &= \frac{1}{W_s}\int_{W_s} H_c(f)e^{j2\pi f\tau}df \\ &\approx \frac{1}{N}\sum_{k=0}^{N-1} H_c(k\Delta f)e^{j2\pi k\Delta f\tau} \end{aligned} \tag{3.2}$$

where W_s is the width of the Blackman-Harris window and $\Delta f = \frac{W_s}{N}$. By letting $\tau = m\Delta\tau = m/W_s$ we obtain the discrete samples of the channel impulse response as

$$h_c(m) = \frac{1}{N}\sum_{k=0}^{N-1} H_c(k\Delta f)e^{j2\pi\frac{km}{N}}, \qquad m = 0, 1, \cdots, N-1 \tag{3.3}$$

Radio channels are usually modeled as wide sense stationary with uncorrelated scattering with the power delay profile (PDP), which is the expected power per unit of time received with a certain excess delay. The PDP is defined as the autocorrelation function of the channel impulse response and can be written as

$$\phi_h(\tau) = E\{h_c(\tau_1 + \tau)\, h_c^*(\tau_1)\} \tag{3.4}$$

where $E\{\cdot\}$ represents the expected value.

Furthermore, to obtain quantitative parameters of the time spread in the environment, the mean excess delay (τ_{mean}) and rms delay spread (τ_{rms}) can be obtained from the averaged PDP in the same position [24]. To estimate the different quantitative parameters, a threshold needs to be set to distinguish the multi-path components from the noise floor. In this case, this threshold, Th_D, corresponds to the $\mu + 3\sigma$ of the noise part, where μ and σ are the mean and variance, respectively. The mean excess delay is the first moment of the power delay profile of the channel and is defined as

$$\tau_{mean} = \frac{\sum_k \phi_h(k\Delta\tau)k\Delta\tau}{\sum_k \phi_h(k\Delta\tau)} \tag{3.5}$$

where k corresponds to the samples above the threshold Th_D.

The rms delay spread is the square root of the second moment of the PDP and is defined as

$$\tau_{rms} = \sqrt{\left(\frac{\sum_k \phi_h(k\Delta\tau)(k\Delta\tau)^2}{\sum_k \phi_h(k\Delta\tau)}\right) - (\tau_{mean})^2} \tag{3.6}$$

The maximum excess delay is the time spread during multi-path components are above a certain threshold and is defined as

$$M_D = \tau_{\max} - \tau_{\min} \tag{3.7}$$

where $\tau_{\min}$ and $\tau_{\max}$ are the arrival time of the first and the last multi-path components, respectively.

The coherence bandwidth is a statistical parameter that defines whether the channel can be assumed as frequency non-selective (flat) or frequency selective over a given frequency band. For a frequency correlation of 0.5 [31, 32], the coherence bandwidth is computed from the τ_{rms} as

$$B_m = \frac{1}{5\tau_{rms}} \tag{3.8}$$

3.2.1 Channel Models

Multiple models have been elaborated in previous works to describe the impulse response of a channel. In this thesis, we take the extended indoor propagation models, Saleh-Valenzuela and IPDP to study the behavior of the various measured and simulated environments.

Saleh-Valenzuela

The Saleh-Valenzuela model divides the impulse response into groups of multi-path rays called clusters [33]. These clusters are distinguished by their separation in time and the power decaying exponentially in each cluster. Figure 3.1 shows the wide-band impulse response of the channel.

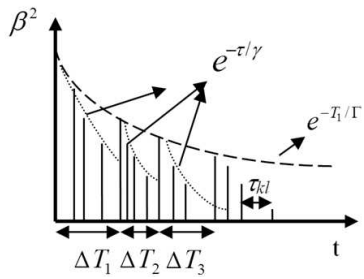

Figure 3.1: Saleh-Valenzuela impulse response model.

The impulse response of the Saleh-Valenzuela model is defined as

$$h(\tau) = \sum_{l=0}^{L-1} \sum_{k=0}^{K-1} \beta_{kl} e^{j\theta_{kl}} \delta(\tau - T_l - \tau_{kl}) \tag{3.9}$$

where L is the maximum number of clusters, K refers to the number of multi-path components in each cluster, β_{kl} and θ_{kl} are the amplitude and the phase of the kth component in

the lth cluster, T_l is the arrival time of the lth cluster and τ_{kl} is the arrival time delay of the kth ray in the lth cluster with respect to the first ray of the lth cluster. And β_{kl} is defined as

$$\overline{\beta_{kl}^2} = \overline{\beta^2(0,0)} e^{-T_l/\Gamma} e^{-\tau_{kl}/\gamma} \tag{3.10}$$

where Γ and γ are the exponential cluster decay and ray decay inside the cluster, respectively, and $\overline{\beta^2(0,0)}$ is the average power of the first component received.

In order to estimate the parameters of Saleh-Valenzuela model, we have used a visual curve-fitting, which is one of the best ways to assess the composition of the PDP. The steps for estimating the S-V model parameters are as follows:

1. Divide the $PDPs$ into clusters.
2. Determine the inter-arrival times (ΔT_l) for every cluster and then average $\overline{\Delta T_l}$ for all $PDPs$ in the same location.
3. Obtain the average ray arrival time, $\overline{\tau_{kl}}$.
4. Determine the average cluster decay constant, $\overline{\Gamma}$, fitting the maximum power of each cluster to an exponential function.

The ray decay constant, γ, is estimated from the modified Saleh-Valenzuela model [21] adopted by the IEEE 802.15.4a channel model in which it is defined that the ray decay constant experiences a higher decay as the delay of a cluster increases. The ray decay constant is defined as

$$\gamma(\tau) = a\tau + \gamma_0 \tag{3.11}$$

where a and γ_0 are constants which depend on the environment, whether there is a line-of-sight path or not.

IPDP Model

The in-room power delay profile (IPDP) is a prediction model used to estimate the behavior of a channel based on the dimensions and materials of the environment [34]. The model defines the power delay profile of the channel as a composition of multiple multi-path components with different amplitudes and delays

$$\phi(m) = \Psi_m \delta(t - \tau_m), \qquad m = 0, 1, \cdots, M-1. \tag{3.12}$$

where M, Ψ_m, τ_m are the number, amplitude and delay of the multi-path components respectively. In order to normalize the power delay profile and set the first component at zero $\Psi_0 = 1$ and $\tau_0 = 0$, the rest of the components Ψ_m and τ_m are defined as

$$\Psi_m = \frac{1}{4}\frac{\gamma^m}{m^2}, \qquad m = 1, 2, \cdots, M-1. \tag{3.13}$$

$$\tau_m = \frac{t_c}{2}(2m-1), \qquad m = 1, 2, \cdots, M-1. \tag{3.14}$$

where γ is the average power reflection coefficient and t_c is the characteristic time of the channel. In real environments where there are multiple surface with different materials γ becomes

$$\gamma_{eff} = 1 - \alpha_{eff} \tag{3.15}$$

where α_{eff} can be defined as

$$\alpha_{eff} = \frac{\sum_{u=1}^{U} S_u \alpha_u}{S} \tag{3.16}$$

where U is the number of surfaces, S is the total surface area in the environment,α_u and S_u are the absorption coefficient and surface area of u respectively.

The characteristic time of the channel, t_c, is defined as

$$t_c = \frac{8V}{cS} \tag{3.17}$$

where V is the volume of the environment and c is the speed of light.

3.3 Measurement Results and Analysis

Industrial environments are often classified as reflective with high multi-path levels; however, from the measurement campaigns performed in multiple environments, we found significant diversity in the channel behavior. Based on our studies, the response of the channel varies from high to low delay spread environments. This section describes the measurement results from the bark furnace, paper warehouse and mine tunnel presented in Chapter 2, ranging over different delay spread levels. The measurement setup based on the network analyzer presented in Chapter 2 is used to obtain the channel impulse response and compute the quantitative parameters of the delay spread.

3.3.1 High delay spread environments

Environments that exhibit high delay spread are environments containing large quantities of metallic materials. This type of environment could correspond to the highly reflective environments, i.e., bark furnace, described in Chapter 2. The work presented in this section is the result of Papers [J2], [J3] and [J4].

By using the measurement setup and by processing the channel response, the PDP can be determined for this environment. The results show that the channel introduces a high level of time dispersion to the signal. Figure 3.2 shows samples of power delay profiles for three different frequency bands in one of the locations in Figure 2.1. We can see that the rms delay spread for a highly reflective environment is greater than 290 ns in some cases, as we reported in Paper [J3]. This shows that a number of industrial environments can exhibit higher rms delay spread levels compared with previous works reported in similar reflective environments [21].

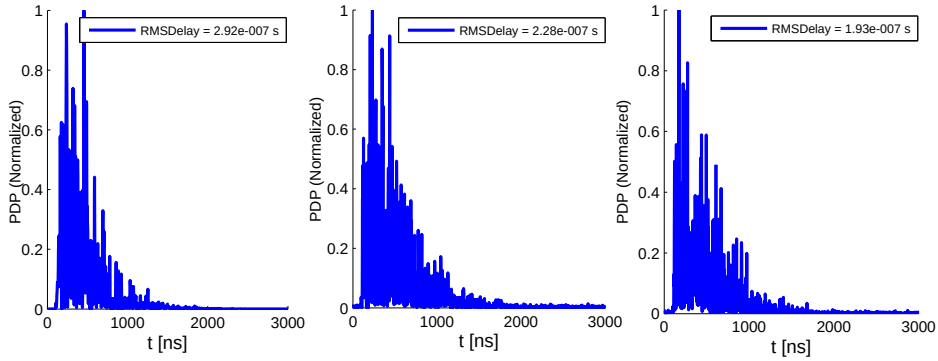

Figure 3.2: PDP at 433 MHz (left), at 1890 MHz (center) and at 2450 MHz (right), NLoS case.

From the PDP, a number of quantitative parameters can be calculated based on the expressions in (3.6), (3.7) and (3.8). Table 3.1 presents a number of results extracted from the measurements. The number of components in the PDP corresponds to the number of paths that the signal takes from transmitter to receiver, for a 2 ns time resolution. We can observe high values of rms delay as well as a maximum excess delay with narrow coherence bandwidth.

Table 3.1: PDP parameters for high delay spread environments

	LoS	NLoS
N° Components	60-223	102-230
τ_{rms} [ns]	178	251
M_D [ns]	244	1020
B_m [kHz]	1123	796

This high delay spread environments can present problems when using a system with a bandwidth higher than the coherence bandwidth. As an example of a common system used in an industrial environment, the DECT system has a channel bandwidth of 1186 kHz. DECT could experience ISI in these high delay spread industrial environments. However, selecting robust systems against ISI, such as WLAN which is based on OFDM, could increase the overall system performance.

3.3.2 Low delay spread environments

Low delay spread environments can be divided in two groups; environments containing absorbent materials and tunnel environments. The first group corresponds to a building with large dimensions containing absorbent elements, i.e., the paper warehouse described in Chapter 2.

The measurement results indicate the absence of multi-path reflections in this environment, in contrast with previous measurement campaigns performed in industrial environments such as [21]. The PDPs for three different frequency bands in the warehouse of paper rolls are presented in Figure 3.3. We observe a difference in the noise floor for the 2450 MHz frequency band, finding that the signal-to-noise ratio is low even at a distance of 6 m between the transmitter and receiver in the NLoS case. Only one main component and a few small reflections are observed as reported in Papers [J3] and [C2]. The rms delay spread calculated is smaller than values that are typical for indoor environments, such as offices [25].

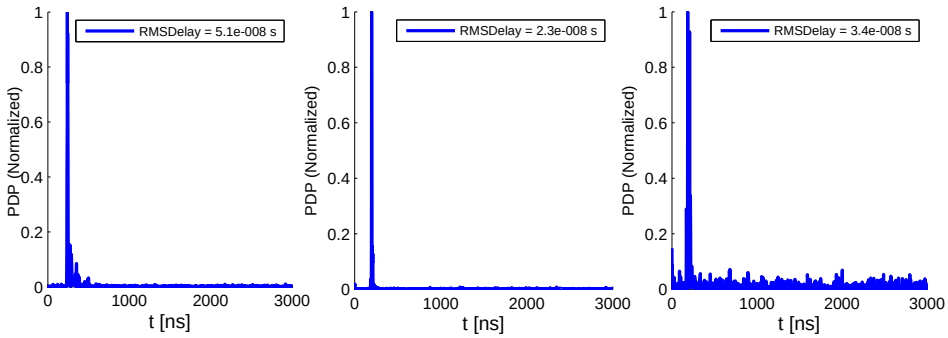

Figure 3.3: PDP at 433 MHz (left), at 1890 MHz (center) and at 2450 MHz (right), NLoS case in the paper warehouse.

Ray tracing software is useful tool for simulating the propagation characteristics of an environment in which it is not possible to perform measurements. In this thesis, we present the simulations for the paper warehouse. The results obtained by the ray trace simulation tool are compared with the measurements, as shown in Figure 3.4 (left). The ray trace simulation is useful tool for determining the multi-path characteristics of industrial environments due to the similarities between the measurements and simulated results. In Figure 3.4 (right), the simulated results obtained with a large number of receivers provide insight into the rms delay spread distribution in the environment.

The second group of low delay spreads corresponds to tunnel environments. Papers [J1] and [C4] contain the main contribution of the tunnel environments. In particular, the results of this part correspond to the mine tunnel environment described in Chapter 2.

From the measurement results in the mine, we can classify the environment as a low-delay spread. Measurement campaigns performed by other authors have reported similar tendencies [28, 29]. Figure 3.5 shows the measured and simulated PDP at 1890 MHz for the LoS scenario. The PDP contains few multi-path components, as in the paper warehouse scenario, due to multi-path components not reflecting on the back of the transmitter and receiver antennas.

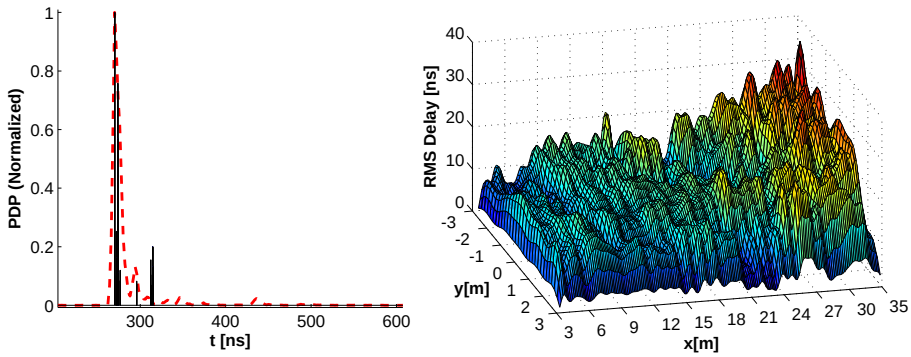

Figure 3.4: Measured and simulated PDP for 433 MHz for the LoS (left) and distribution of rms delay spread in the receiver simulated grid (right), in the paper warehouse.

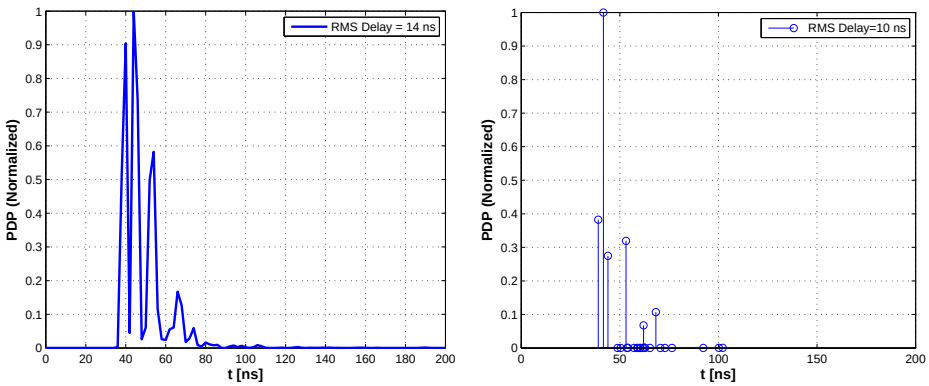

Figure 3.5: Measured (left) and simulated (right) PDP at 1890 MHz for the LoS in the mine tunnel.

Table 3.2 lists a number of quantitative parameters related to the low delay spread environments. We identify fewer than 27 components in the PDPs. The maximum excess delay is not greater than 31 ns for the NLoS cases.

This low delay spread environment should not produce ISI in actual wireless systems. The selection of systems based on OFDM technology to cope with the multi-path degradation is therefore not necessary.

Table 3.2: PDP parameters for a low delay spread environment

	LoS	NLoS
Nº Components	9-27	5-19
τ_{rms} [ns]	11	28
M_D [ns]	16	31
B_m [kHz]	18181	7142

3.3.3 Channel Model Results

This section is based on the work performed in Papers [C3] and [J3]. In Paper [C3], the IPDP is analyzed with respect to other propagation models. Paper [J3] contains a comparison between the two industrial environments that exhibit different propagation behavior, i.e., reflective and absorbent, with the extracted Saleh-Valenzuela model parameters.

Saleh-Valenzuela Model

We can observe the averaged extracted parameters of the high and low delay spread environment in Table 3.3. The results are obtained by averaging seven PDPs in 16 locations. In the low delay spread environment, the presence of a single cluster makes the estimation of most of the parameters impossible. This problem with the cluster division has also been noticed in reflective environments such as those in [21].

Table 3.3: Channel parameters of the Saleh-Valenzuela model

	LoS High Delay Spread	LoS Low Delay Spread
$\overline{\Delta T_l}$ [ns]	40.1	-
$\overline{\tau_{kl}}$ [ns]	6.7	5.8
$\overline{\Gamma}$ [ns]	187.3	8.9
γ_0	7.64	-
a	0.93	-

The estimated parameters of the Saleh-Valenzuela model are validated by simulating the PDP and computing the rms delay spread. In Figure 3.6, we can observe the simulated and measured PDPs in the high delay spread environment for the LoS scenario. The simulated and measured rms delay values are within the same range, showing high delay spread behavior in the environment.

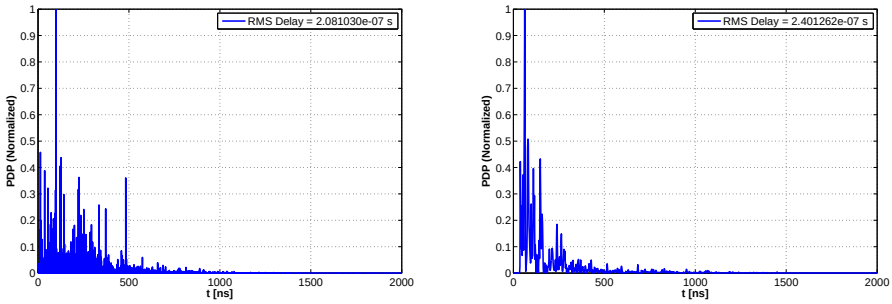

Figure 3.6: Simulated Saleh-Valenzuela PDP (left) and measured PDP (right) in high delay spread environment.

IPDP Model

Upon setting the properties of the building structure and the reflection coefficient in both environments, the PDP was computed. Figure 3.7 shows the simulated power delay profile of the high and low delay spread environments described previously. The simulations are within the range of the measurements results from the previous sections.

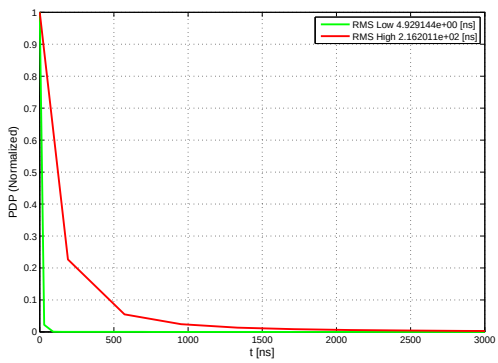

Figure 3.7: PDP of the IPDP model for low and high delay spread channels.

3.4 Discussion

This chapter described a characterization of the multi-path propagation in diverse industrial environments. Previous studies define industrial environments as high delay spread environments caused by the building structure and metallic elements present in the environment. In this chapter, we characterize environments with different delay spreads,

distinguishing between high and low delay spread. The multi-path characterization and spread delay quantification carried out in the diverse industrial environments is a product of a developed delay spread measurement setup. The impulse responses of the characterized industrial environments are modeled using the Saleh-Valenzuela and IPDP channel models. The distinction of industrial environments behaving in different manners could result in the awareness of the system developers to produce adaptive wireless systems that could exploit the propagation properties of the channel, increasing the reliability of the communication system.

Chapter 4

Path Loss Characterization in Industrial Environments

4.1 Introduction

Radio waves experience different types of fading effects in industrial environments. The previous chapter described the short-term fading effects referred to as multi-path fading. This chapter focuses on the long-term deterministic path loss. Path loss describes the variation of the signal strength over large distances on wide frequency bands. The path loss is usually analyzed with respect to the distance for a narrow frequency band. For instance, an extensive measurement campaign carried out in residential and commercial areas performed by Ghassemzadeh *et al.* [26] showed path loss exponents, i.e., distance dependence, with values ranging from 1.35 to 2.38. A study in office environments at 5.3 GHz showed similar tendency, with path loss exponents equal to 1.3 and 2.9 for LoS and NLoS scenarios, respectively [25].

Multiple measurements have been taken to investigate the distance dependence of the radio propagation in industrial environments. Three measurement campaigns at 900, 2400 and 5200 MHz using narrow-band receivers found path loss exponents lower than the corresponding free space, i.e., $\alpha = 2$ [9, 10, 23]. Rappaport performed a measurement campaign at 1.3 GHz in an automation factory, and four additional industrial environments reporting a path loss exponent ranging between 1.49 and 2.81 [35].

Regarding the frequency dependence of the path loss, an overview of a path loss frequency dependence following a simple power law or exponential function is presented in [36]. The well-known empirical models designed for predicting the propagation in urban, suburban and rural areas, i.e., the Okumura-Hata model, contain a frequency dependence in the propagation models [37, 38]. Furthermore, an extension of this model to increase the frequency band up to 2 GHz is reported in the COST 231-Hata model [39]. Path loss measurements in a residential area are reporting a frequency dependence in their results [40]. In [41], a prediction of the frequency dependence in rural and urban areas found a frequency exponent between $\pm$ 0.2 and $\pm$ 1.5. Other measurement campaigns

in urban areas studying the frequency dependence produced by the heights of houses and trees reported that the frequency exponent is between 2 and 3 [42]. A study of the path loss in a multiband channel inside a corridor and a hall reported a frequency exponent with values ranging between 1 and 4 [43].

Few measurement campaigns have investigated the path loss frequency dependence in industrial environments. The IEEE 802.15.4a report [44] presents a path loss frequency dependence following a power law and the extracted parameters of path loss, multi-path and shadowing models in multiple environments. This work reports a frequency exponent value of 1.103 and 1.427 for LoS and NLoS scenarios, respectively.

This chapter discusses the path loss in reflective and absorbent industrial environments and extracts the path loss exponent and the frequency exponent parameters used to describe the propagation channel behavior in these environments. The content of this chapter is based on the measurement results performed in Paper [J3]. The next section of this chapter presents the theoretical background. The third section contains the results obtained in the measurements and the model parameters that describe the behavior of the environment. The last section presents a discussion of the work performed in this chapter.

4.2 Path Loss in Wireless Communications

The free space propagation is a general model used to estimate the performance of wireless links. To characterize the path loss in the environment, we start by defining the free space propagation model in a line-of-sight scenario. The path loss can be expressed as a function of the transmitted, received signal or the Friis free space model [24] as defined

$$\begin{aligned} L_P(d,f) &= P_{Tx}(f) - P_{Rx}(d,f) \\ &= -G_{Tx}(f) - \eta_{Tx}(f) - G_{Rx}(f) - \eta_{Rx}(f) + 10\log_{10}\left(\frac{\lambda}{4\pi d}\right)^2 \end{aligned} \quad (4.1)$$

where P_{Tx} and P_{Rx} are the power of the transmitter and receiver, respectively, G_{Tx} and G_{Rx} are the antenna gains of the transmitter and receiver, respectively, η_{Tx} and η_{Rx} are the antenna efficiency of the transmitter and receiver, λ is the wavelength and d is the distance between the transmitter and receiver.

As a practical approach when performing measurements near the ground and in environments with many obstacles, the path loss can be written in its general form as follows [44, 45]

$$L_P(d,f) = P_{Rx}(d,f) - P_{Rx}(d_0,f) + L_{P0}(d_0,f) \quad (4.2)$$

where $P_{Rx}(d_0,f)$ and $P_{Rx}(d,f)$ represent the received power on the frequency, f, and distance d_0 and d respectively. In this way, the effect of the antennas, i.e., the antenna gains, antenna efficiencies, and transmission power are calibrated. The $L_{P0}(d_0,f)$ is the Friss free space path loss at distance d_0 obtained as

$$L_{P0}(d_0,f) = 10\beta\log_{10}(f) + 10\alpha\log_{10}(d_0) + A + 10\log_{10}\left(\frac{4\pi}{c}\right)^2 \quad (4.3)$$

where β is the frequency exponent of the path loss, α is the path loss exponent (distance exponent), A is a constant varying for LoS and NLoS scenarios, and c is the speed of light.

For a d_0 and f given in meters and MHz respectively, then (4.3) can be formulated as

$$L_{P0}(d_0, f) = 10\beta \log_{10}(f) + 10\alpha \log_{10}(d_0) + A + -27,558 \tag{4.4}$$

As we can see in (4.4), the path loss is composed by four terms; frequency dependent term, distance dependent term and two constants.

The frequency exponent, β, can be extracted from the path loss by taking the derivative of the path loss at distance d with respect to the frequency in dB as

$$\beta = \frac{1}{10} \frac{dL_P(f)}{d \log_{10}(f)} \tag{4.5}$$

4.3 Measurement Results and Analysis

In this section, we present the measurement results and analysis obtained in the bark furnace, i.e., reflective, and paper warehouse, i.e., absorbent, environments described in Chapter 2. The setup to obtain the path loss in the frequency band between 200 and 2500 MHz is based on the generic spectrum analyzer setup presented in Chapter 2. In this case, the measurement setup is composed of a signal generator, spectrum analyzer and three broadband antennas. The signal generator transmits a continuous wave using a broadband directional antenna. At the receiver, two antennas separated by at least $\lambda/2$ are deployed to reduce the small-scale fading and the shadowing degradations providing a global mean. The combined signal from the two antennas is fed into the spectrum analyzer and transferred to the computer. The measurement results of this chapter are product of the work performed in Paper [J3]; however, an extension has been performed to clarify the frequency dependence in the NLoS scenario.

Absorbent and reflective environments behave differently from each other, producing distinct path loss results. To describe the behavior of the environment, we start by not considering the frequency exponent of the path loss in the free space model (4.4). Thus, the frequency exponent $\beta = 2$ is selected, and the path loss exponents for the different cases are extracted by least squares. For this purpose, the figure of merit used for estimating the path loss exponent is the mean square error (MSE). In Table 4.1, we can observe the estimated path loss exponents for the reflective and absorbent environments in LoS and NLoS scenarios. The path loss measurements are performed in the 200 to 2500 MHz frequency range, with a separation distance $d = 9$ m between the transmitter and receiver antennas and the antennas mounted at a 1.5 m height. The NLoS scenarios exhibit higher path loss exponents relative to the values observed in the LoS scenario as could be expected.

The measurements of the path loss with respect to the frequency at a distance $d = 9$ m in the LoS and NLoS scenarios are illustrated in Figure 4.1. The left figure shows the LoS measurements for the absorbent and reflective environments with the free space model for $\alpha = 2$. The right figure illustrates the NLoS situation with the corresponding free space model curves for the extracted α values in each scenario. The LoS scenario follows the

Table 4.1: Path loss exponents for the absorbent and reflective environments

	LoS	NLoS
Absorbent	1.99	2.39
Reflective	1.86	2.54

free space model; however, the corresponding free space model for the NLoS scenarios is not a representative case for describing the measured results. The measurements show a frequency dependence not described properly by the free space model in (4.4).

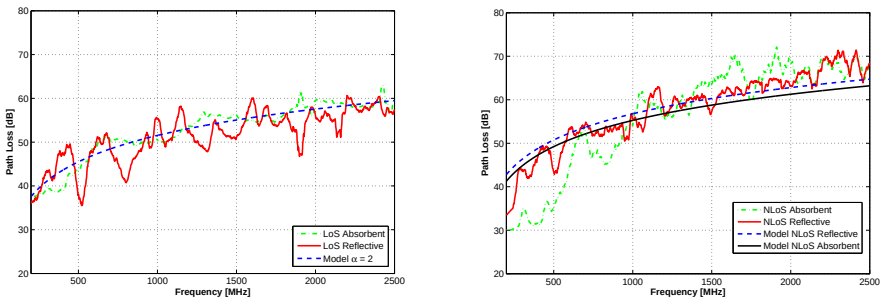

Figure 4.1: Path loss versus frequency of the measurements at 9 m in absorbent and reflective for LoS (left), NLoS (right) and the theoretical estimation for a $\beta = 2$.

To provide a model that describes the path loss in NLoS situations, the frequency exponent, β, is estimated for the different scenarios (4.4). To obtain this frequency exponent, β, the derivatives of the measured path loss are extracted. Figure 4.2 illustrates the derivatives of the path loss in the different scenarios, showing that the derivatives are constants and fluctuate between environments. By extracting the sample mean value of these derivatives, the frequency exponent, β, is estimated.

Table 4.2 provides the estimated parameters of the path loss model with the frequency exponent (4.4). The frequency exponent, β, is higher in the NLoS scenario than in the LoS scenario. Within all the environments, the absorbent environment in the NLoS scenario presents the highest frequency exponent. This strong frequency dependence is supposed to be related to the physical properties (permittivity, conductivity) of the material stored in the environment, i.e., the paper rolls. The estimated frequency exponent in industrial environments is higher than the value reported in [44], especially for NLoS scenarios in the absorbent environment.

Figure 4.3 shows the NLoS measurement with the path loss estimations, taking into account the frequency exponent. The estimated curves describe the behavior of the environments more efficiently than in the case where the frequency exponent is fixed to $\beta = 2$.

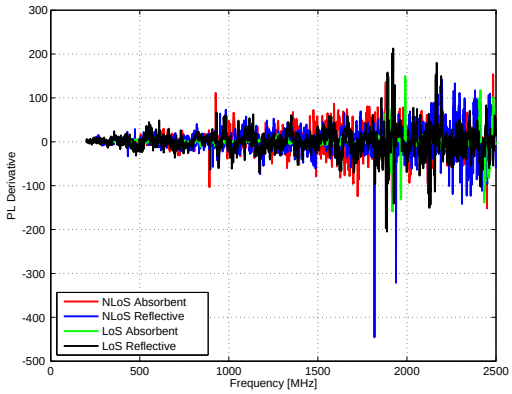

Figure 4.2: Derivatives of path loss in absorbent and reflective environments in LoS and NLoS.

Table 4.2: Estimated parameters for LoS and NLoS in the absorbent and reflective environments with a path loss model containing frequency exponent.

	LoS			**NLoS**		
	α	β	A	α	β	A
Absorbent	1.99	2.00	0.01	2.39	3.78	54.88
Reflective	1.86	1.82	-5.03	2.54	3.02	31.33

Table 4.3 contains the MSE between the estimation and the measurement for all the different cases. The LoS scenario does not exhibit an improvement when applying a path loss model with the frequency exponent. However, the MSE for the NLoS scenarios decreases substantially. The MSE decreases by approximately 38 dB in the absorbent environment when using the path loss model of (4.4).

Table 4.3: MSE[dB] of the estimations for LoS, NLoS in the absorbent and reflective environments

	LoS		**NLoS**	
	LoS	LoS Freq Exp	NLoS	NLoS Freq Exp
Absorbent	2.68	2.34	50.24	12.65
Reflective	9.86	9.52	10.39	4.38

To provide an overall environment comparison, the resulting estimated path loss curves for the LoS and NLoS scenarios in the absorbent and reflective environments are presented in Figure 4.4. The figure shows a strong frequency dependence for the NLoS scenarios, in particular for the absorbent environment.

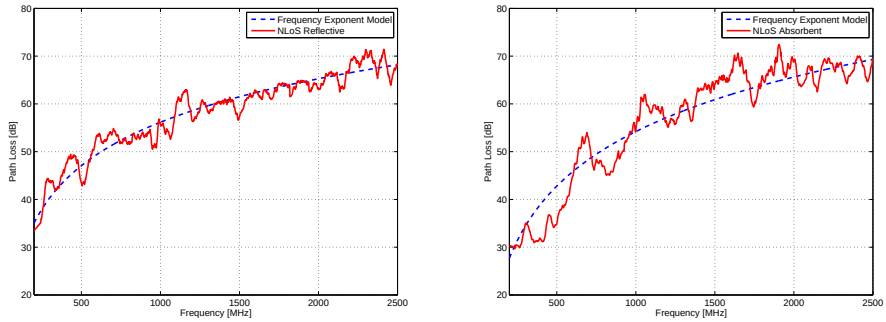

Figure 4.3: Path loss versus frequency of the measurements in NLoS for absorbent (left), reflective (right) and the theoretical estimation with the frequency exponent model at 9 m.

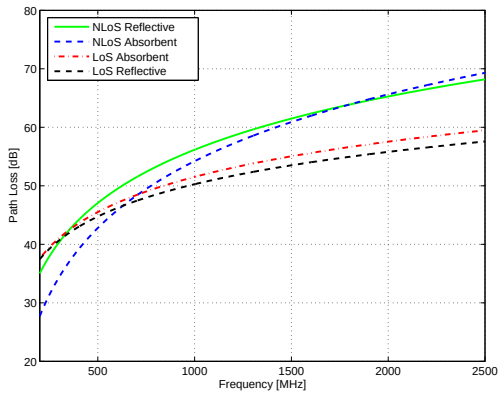

Figure 4.4: Estimated theoretical path loss in absorbent and reflective environments in LoS and NLoS.

4.4 Discussion

In this chapter, the long-term deterministic path loss was studied in absorbent and reflective industrial environments. This chapter focused particularly on studying the frequency dependence of the path loss in industrial environments. To characterize the path loss, a measurement campaign was carried out in different locations in these absorbent and reflective environments. An asynchronous setup composed of a SG and SA was used to scan the channel and obtain the path loss characteristics. By analyzing the measurement results, a frequency dependence can be observed, and consequently, a model with a frequency exponent is used to describe the channel behavior. The results show a path loss exponent

with values ranging between 1.86 and 2.54 in the LoS and NLoS scenarios, respectively. Regarding the frequency dependence path loss, the frequency exponent in the NLoS scenarios is two times the frequency exponent estimated in the LoS scenarios. In particular, the absorbent environment in the NLoS scenario presents the highest frequency exponent, obtaining values up to 3.78. This result indicates a stronger frequency dependence than the frequency dependence reported in previous studies for industrial environments.

Chapter 5

Electromagnetic Interference in Industrial Environments

5.1 Introduction

Electromagnetic interference (EMI) or man-made interference is one of the most problematic electromagnetic degradations sources that wireless systems must address in industrial environments. EMI is produced by different sources, such as electric motors, repair work, fluorescent tubes and machinery [5]. Man-made interference or EMI decreases the reliability of communications. While such reduced reliability may be acceptable in most wireless systems deployed in office or residential environments, a reliability reduction is not suitable for industrial communications. Industrial processes require robust and reliable communications with a failure probability that is almost negligible.

Many research groups have detected and characterized EMI present in industrial environments [46, 47]. A survey performed in [11] presents the most common sources of interference in industrial environments: electric motors, ignition systems, welding processes, rectifiers, power lines and switching devices. This survey provides the frequency signature of these interference sources and shows that interference from a welding process appears at frequencies lower than 100 MHz. E. N. Skomal also investigated the radiating interference of welders and power lines, showing similar results [12]. Moreover, the authors in [48] measured and modeled the interference produced by a modern electric motor, extracting the high-frequency model parameters with a network analyzer.

Furthermore, a number of electrically powered transportation systems in industrial environments need to be considered when characterizing the different sources of interference. For instance, the work performed in [49] studied interference from a motorcycle and proposed a cancellation technique by implementing a multilayer perceptron (MLP) neural network. EMI from electric trains was studied in [50], the authors reported malfunction of pacemakers in high-speed trains caused by the inductive coil filter of the electrical system. Moreover, an investigation performed in [51] showed the presence of electromagnetic fields when the train enters in the powered sections where the batteries are charged from

the overhead power lines.

Recent studies consider the amplitude probability distribution (APD), also known as the complementary cumulative distribution function, as a statistical method for characterizing EMI [52–54]. In [55, 56], the authors make use of the APD to estimate the impact of an interference signal from a microwave oven on several modulation schemes. Studies of multichannel analyses using APD measurements have been performed [57, 58]. However, these measurement techniques have only been used in laboratory environments to characterize the properties of the interference source.

This chapter presents an EMI characterization and APD analysis in the broad frequency band between 20 and 3000 MHz in industrial environments based on Papers [C1], [J1], [J2] and [J4]. Many sources of interference are found in different industrial environments, such as in the bark furnace, outdoors, rail yard and iron-mine tunnel environments described in Chapter 2. From the captured EMI, we aim to characterize and model the statistical parameters of the EMI, studying the performance of wireless systems under such EMI.

The next section presents the theoretical model that describes the EMI and the EMI identification through an APD analysis. The third section contains the measurement results of the EMI produced by different sources. The last section gives a discussion of the work performed in this chapter.

5.2 Electromagnetic Interference Model

To study the impact of EMI in a communication system, interference models need to be defined. Previous studies have captured EMI by analyzing and estimating the model behavior, such as with Middleton's models [59, 60]. Middleton's models depending of the relation between the interference and signal bandwidth are divided in three classes A, B and C. The amplitude probability density function of a class A model is defined as

$$f_x(x) = e^{-A} \sum_{m=0}^{\infty} \frac{A^m}{m!\sqrt{2\pi\sigma_m^2}} e^{-\frac{x^2}{2\sigma_m^2}} \tag{5.1}$$

where m is the number of interfering signals, Γ is the power ratio between the Gaussian and non-Gaussian components, A corresponds to the duration of an impulse multiplied by the number of impulses per unit time, and σ_m^2 is defined

$$\sigma_m^2 = \frac{\frac{m}{A} + \Gamma}{1 + \Gamma} \tag{5.2}$$

Middleton's parameters model can be estimated following the study in [61].

The Middleton model defines the EMI as a composition of Gaussian noise and non-Gaussian noise. In this work, we are interested in working with Gaussian and non-Gaussian noise (particularly impulsive noise) individually for detection and suppression purposes as will be studied in Chapter 7. Thus, this thesis makes use of a system where the received signal is composed of a transmitted signal, Gaussian noise and impulsive noise separately [62, 63]. Hence, the low-pass received signal can be defined by

$$r(t) = s(t) + w(t) + i(t) \tag{5.3}$$

where $s(t)$ is the transmitted signal, $w(t)$ corresponds to a Gaussian noise process with zero-mean and σ_w^2 power spectral density, and $i(t)$ is the impulsive noise part defined as

$$i(t) = \sum_{i=-\infty}^{+\infty} A_i B_w \delta(t - b_i) \tag{5.4}$$

where A_i is the frequency amplitude of the impulse i which can be considered to be flat in the receiving bandwidth [16], B_w, and b_i is the arrival time of the impulsive noise i following a Poisson process [64] with a given arrival rate λ; i.e., the probability of x events arriving in t units of time has a distribution

$$P(x) = \frac{\lambda^x e^{-\lambda}}{x!} \tag{5.5}$$

At this point, sampling the received signal at the sampling rate T_s, the discrete received signal can be formulated as

$$r_n = r(nT_s) = s(nT_s) + w(nT_s) + i(nT_s) \tag{5.6}$$

To quantify how harmful the impulsive noise is, we would like to define the impulsive rate and the impulsive power. The impulsive rate, IR, provides the ratio between the number of disturbed samples and the total number of received samples and is defined as

$$IR = \frac{\sum_{n=1}^{N_t} P\left(\mid r_n \mid > Th\right)}{N_t} \tag{5.7}$$

where Th is the threshold selected to classify a sample as impulsive or not, in Chapter 7 we will show different methods for selecting this threshold, N_t is the total number of observed samples, and

$$P\left(\mid r_n \mid > Th\right) = \begin{cases} 1, & \mid r_n \mid > Th \\ 0, & \text{otherwise} \end{cases} \tag{5.8}$$

The relation between the average power of the impulses, the signal and the additive white Gaussian noise is defined as follows

$$\Gamma = \frac{\sigma_i^2}{\sigma_s^2 + \sigma_w^2} \tag{5.9}$$

where σ_i^2, σ_s^2 and σ_w^2 are the power spectral densities of the impulsive noise, signal and additive white noise, respectively.

5.2.1 Amplitude Probability Distribution

The APD has been widely used to represent and visualize statistically EMI [52]. Thus, the APD is a performance measure of EMI in an environment. The APD of the captured signal can be defined as the probability that a random amplitude X exceeds a certain amplitude x_0

$$\mathrm{APD}(x_0) = \Pr\left[X > x_0\right] = 1 - F(x_0) \tag{5.10}$$

where $F(x_0)$ is the cumulative distribution function (CDF) of X.

For instance, Figure 5.1 (left) illustrates the amplitude of a received signal containing impulsive noise and a signal free of impulsive noise. The APD representations for these cases are shown in Figure 5.1 (right). The received signal containing impulsive noise is composed of two regions; the first region, i.e., no impulsive noise, where the $s_n + w_n$ dominates, and the second region, i.e., impulsive noise region, where the impulsive noise dominates. Thus, the APD representation of the received signal can be used to visualize the presence of impulsive noise and to estimate the threshold, Th, for detecting and suppressing the impulsive noise as will be investigated in Chapter 7.

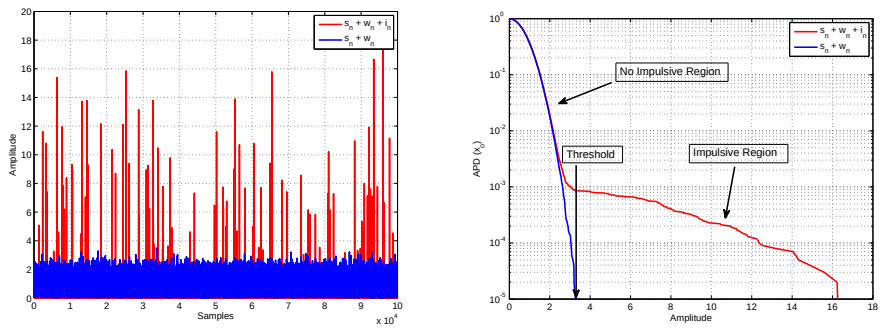

Figure 5.1: Time domain measurement (left) and APD of the data (right).

5.3 Measurement Results and Analysis

An electromagnetic characterization of a wide-band spectrum was performed in the bark furnace environment presented in Chapter 2, also known as highly reflective environment. This characterization is reported in Papers [C1], [J2] and [J4], where multiple sources of EMI are captured in a number of industrial environments. The measurement setup used for capturing the EMI is based on the generic spectrum analyzer setup described in Chapter 2. In particular, the setup is composed of a broadband antenna covering frequencies from 20 to 3000 MHz connected to a spectrum analyzer and a computer with a 12-bit analog digital converter (ADC).

The measurement method to capture the EMI is based on the CISPR 16-2-3 [65]. To begin, a wide-band frequency scan is performed to identify the frequency components affected by the interference. The minimum scan time when performing a wide-band frequency scan using video bandwidth wider than RBW can be calculated according to the electromagnetic compatibility (EMC) standard CISPR 16-2-3 [65] by

$$T_{min} = \frac{k_s \Delta f}{(\mathrm{RBW})^2} \tag{5.11}$$

where k_s is related to the resolution bandwidth (RBW) filter shape. The parameter k_s takes on values between 2 and 3 for a Gaussian shape and between 10 and 15 for stagger-tuned filters, and Δf corresponds to the scanned frequency band.

Once the frequency components affected by the EMI are located, a time measurement setting zero-span mode in the SA is used. To prevent distortion in the measurement, the RBW should be set to greater than the analyzed wireless system, and the sampling frequency of the ADC board in the computer should be set to at least 10 times higher than the RBW.

Figure 5.2 (left) shows interference from a process inside the bark furnace environment. The figure illustrates that these impulsive interferences are located within the band from 20 MHz to 2 GHz, where the majority of the industrial wireless communications occur. DECT is a system used for voice and data communications in industrial applications, operating at the 1.8 GHz frequency band. Figure 5.2 (right) shows the interference disturbances captured found in the DECT band. Malfunctioning of the DECT communication systems in this reflective environment was reported by the company. Once the interference is located in the frequency spectrum, a time domain measurement is performed at the affected frequency band to determine the statistical properties of the signal and the interference. The time domain measurement was performed in the DECT band using a peak detector, 30 kHz of RBW and 51 kHz of VBW.

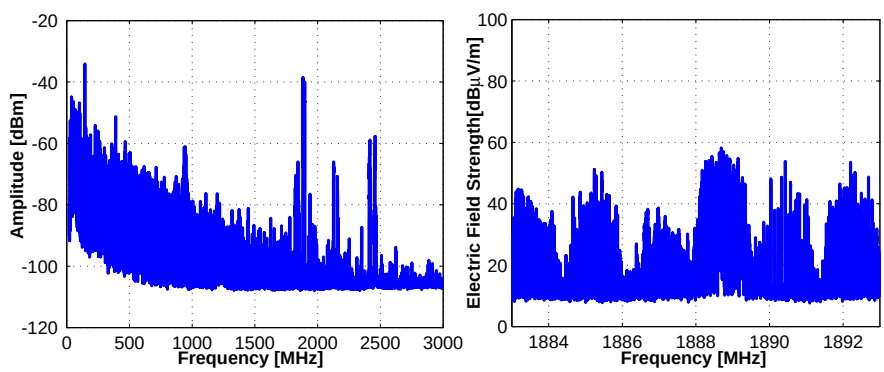

Figure 5.2: Electromagnetic interferences at low frequencies (left) and disturbances on the DECT band (right).

The impulsive rate and the amplitude of the impulses are estimated for the interference captured in time domain. In the absence of wireless systems at the measurement time, to separate the impulsive noise from the background noise, the background noise is assumed to follow a Gaussian distribution with mean, μ, and variance, σ_w. Thus, by setting a decision threshold, Th, to $\mu+4\sigma_w$ the probability that a Gaussian sample has a peak higher than Th is less than 9×10^{-4} [66]. In this way, the impulsive samples and the background noise can be divided into two groups. The estimated parameters for this interference give a $\Gamma = 47.7$ and $IR = 3.17 \times 10^{-2}$. Figure 5.3 shows the APD of both signals, measured and estimated, where the mean square error (MSE) between them is less than 1.28 dB.

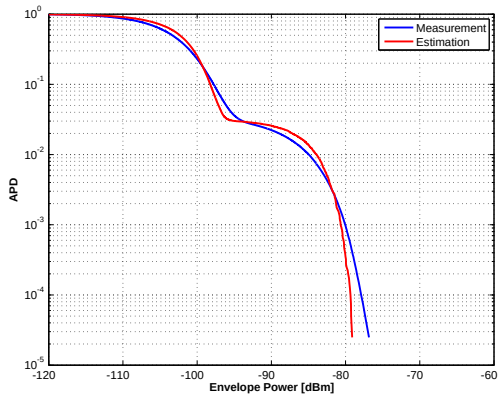

Figure 5.3: APD of the measured interference and the estimated.

In addition to the measurements performed in industrial environments with a large number of metallic surfaces and electric elements, this thesis also examines other alternative sources of disturbances that may appear in industry. Transportation and repair activities performed in industrial environments may generate EMI. For this case, we present the interference caused by trains, mopeds and welding processes.

The measurement results shown in Figure 5.4 (left) correspond to a train driven in the rail yard environment described in Chapter 2. This result is also reported in Paper [J2]. When the train was using the brakes, a considerable increase in the total noise floor within the entire observation frequency band was observed. The electric driven train draws power from the overhead power lines via a pantograph. The design involves the use of inverters that contribute considerably to the measured noise. From the results, we observed that during the braking process, the EMI covered a frequency band from 20 MHz to 2 GHz. The noise floor grew between 5 dB and 20 dB, depending on the frequency, and a number of impulsive peak levels reached 60 dB with respect to the reference measurement.

In Paper [J1], a characterization of the iron-mine presented in Chapter 2 was studied. In this paper, EMI from a train passing by was observed as shown in Figure 5.4 (right). A loaded train inside of the mine introduces EMI within the frequency spectrum of 20 MHz

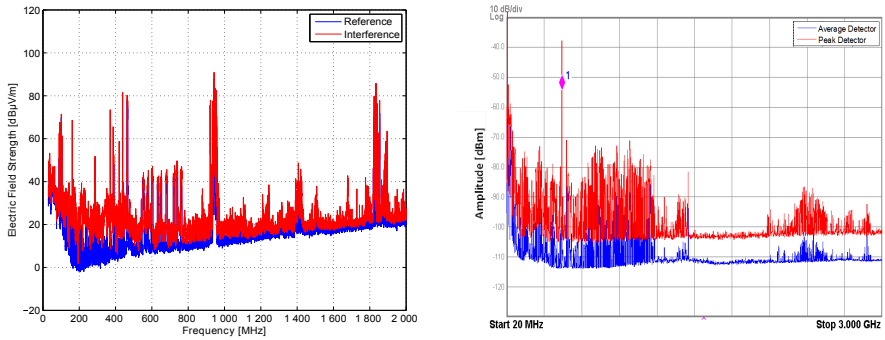

Figure 5.4: Electric train breaking, in Borlänge (left) and in an iron-mine tunnel (right).

to 1.5 GHz with peak levels up to 30 dB. The system developers must be aware of the presence of EMI to design robust wireless systems and avoid possible malfunctions in the communication.

With the introduction of modern transportation using mopeds and four-wheel motorcycles, new disturbances have appeared within existing wireless communication systems in industrial environments. The results captured from a four-wheel moped during the measurement campaign are described in Paper [C1]. These interferences mainly appear within the frequency spectrum from 20 MHz to 1 GHz. The EMI peak levels can reach more than 15 dB higher than the noise floor, and therefore, communication systems operating in this band could experience serious problems in the proximity of moped vehicles.

In industrial environments, welding is an activity commonly performed during repair work and in industrial processes. During the measurements performed in Paper [C1], we captured electromagnetic interferences produced by welding activities. Welding inverters usually present interference levels at frequencies lower than 5 MHz, [67, 68]. During the performed measurement campaigns, the presence of interference was observed at higher frequencies as well, containing frequency components up to 100 MHz.

5.4 Discussion

This chapter discussed the presence of EMI in industrial environments. There are many activities in industrial environments that can cause EMI. This interference can appear in different parts of the frequency spectrum. In our study, we observed EMI at frequencies higher than those reported in the literature. Hence, EMI can be quite harmful to several wireless communication systems in industrial environments. This needs to be taken into consideration when designing and deploying a wireless solution in industrial environments. In fact, by properly characterizing EMI, we acquire additional knowledge on how to design and select wireless technologies with the highest robustness against these interferences. In

addition, increasing our understanding of EMI can decrease the risk of incidents where personnel and materials can be harmed.

Based on the measurement results, we have modeled the observed EMI by extracting its statistical parameters. With these parameters, the impulsive interference can be reproduced and used to investigate the effects of such interference on the performance of wireless communication systems based on the amplitude distribution function. The obtained results showed that EMI degrades the performance of wireless links considerably. Hence, to ensure reliable wireless communications within industrial environments, techniques to mitigate such interference are needed. This performance study is discussed in Chapter 7, where detection and suppression techniques of EMI in industrial environments are introduced and investigated.

Chapter 6

Antenna Systems in Industrial Environments

6.1 Introduction

Reliable communication implies having a wireless link with low probability of failure. As studied in previous chapters, the transmitted signal quality is reduced when encountering channel degradation sources, such as multi-path fading, path loss and interference. A number of approaches can be implemented to increase the signal quality at reception and the reliability of the system, such as spatial diversity, antenna polarization, frequency diversity, channel equalization and interference mitigation. Spatial antenna diversity is an effective technique to combat the fading degradations of the channel and to improve the received signal quality [69]. By using more than one antenna, the receiver is capable of combining multiple signals, thereby obtaining an improved version with lower fading levels. This improvement is dependent on the number of antennas, combining technique used, fading characteristics of the channel and the separation between the antennas.

Chapter 3 discussed industrial environments with high levels of multi-path fading and that consequently provide a potential scenario for implementing spatial antenna diversity. By placing multiple antennas at a certain separation, the receiver will receive uncorrelated multi-path replicas of the signal. By increasing the antenna separation, the receiving signals experience lower cross-correlation and the system provides higher diversity gain. Critical industrial communications require highly reliable levels to operate properly, but physical limitations exist for separating the antennas, by rule of thumb $\lambda/2$, to reach the desired spatial diversity gain. Industrial communication systems often use low frequency bands, such as 433 and 868 MHz, which require a long antenna separation; therefore, a study of spatial diversity must be performed in industrial scenarios at these bands.

Previous studies have investigated the antenna spatial diversity in various environments. In paper [70], the authors investigated the benefits of using more than one receiving antenna. They reduced the fading depth levels by more than 19 dB when using three antennas and adjusting the antenna heights. The authors in [71] investigated the spatial and

polarization diversity efficiency in mobile base-stations, obtaining gains between 5 and 9 dB in the case of polarization diversity and between 6 and 10 dB in the case of spatial diversity. A measurement campaign that developed a smart base-station for measuring the diversity concluded that spatial diversity is more efficient than polarization and angle diversity when the antennas are polarized vertically [72]. A study of the gain when implementing polarization and spatial diversity is reported in [73], where the authors show a diversity gain between 3.5 and 6 dB for spatial and 3 and 5.2 dB for polarization diversity. A paper measuring the correlation coefficient and k-factor in the 902-828 MHz frequency band evaluated the diversity performance of the different combinations of a planar-inverted F antenna (PIFA), helix and monopole in an office environment [74]. The study in [15] carried out an intensive measurement campaign, characterizing the spatial, polarization and pattern diversity in urban, rural, outdoor-to-indoor and indoor environments. This investigation concluded that at 99% reliability, indoor environments exhibit a Ricean k-factor of 0.57 and can provide a diversity gain of up to 9.3 dB.

According to the literature review, few studies have been performed regarding spatial diversity measurements in industrial environments. In this chapter, we study spatial diversity in two industrial environments and in one office environment. This chapter is based on the measurements performed in the industrial environments presented in Paper [J5]. In addition, this chapter presents a measurement in an office corridor together with a diversity gain analysis using selection combining (SC) and maximal ratio combining (MRC) in all the environments.

The content of this chapter is structured as follows. The next section presents the theoretical background, namely, cross-correlation, Ricean k-factor and diversity techniques for obtaining the diversity gain. The measurement results in the two industrial environments and the office corridor are presented in the third section. The last section of this chapter provides a discussion of the overall spatial diversity investigation.

6.2 Spatial Diversity in Wireless Communications

This section describes the theoretical background necessary to understand and quantify the improvement when spatial diversity is implemented. First, the cross-correlation is presented for a system composed of two antennas. Next, the estimation of the Ricean k-factor is described. Finally, the computation of the diversity gain when applying selection combining and maximal ratio combining is presented.

Cross-Correlation

The benefit of the spatial diversity is directly related to the cross-correlations of the received signals in the two antennas, x and y. The cross-correlation of the two continuous functions, x and y, in time domain can be defined as

$$\rho_{xy}(t) = \int_{-\infty}^{\infty} x(\tau - t)y(\tau)d\tau \tag{6.1}$$

For a discretized functions x and y, the normalized cross-correlation can be estimated

as [74].

$$\overline{\rho}_{xy}(n) = \frac{\sum_{n=1}^{N} (x(n) - E[x])\,(y(n) - E[y])}{\sqrt{\sum_{n=1}^{N} (x(n) - E[x])^2 \sum_{n=1}^{N} (y(n) - E[y])^2}} \tag{6.2}$$

where $E[.]$ is the expected value of the corresponding blocks x or y and N is the number of samples of the data blocks.

The cross-correlation of two received signals from two antennas separated by a distance d has been investigated by Clarke [75]. Clarke developed a model describing the cross-correlation of the two received signals when passing through a Rayleigh channel and formulated it as

$$\overline{\rho}_{xy}(d) = J_0^2\left(2\pi\frac{d}{\lambda}\right) \tag{6.3}$$

where J_0 corresponds to the zero-order Bessel function, d is the antenna spacing and λ is the wavelength. The Clarke model is designed for a Rayleigh fading channel being valid for an angle of arrival distributed uniformly in azimuth and with all the antennas identically polarized. This means that the model considers only the multi-path components arriving in a single antenna plane.

Ricean k-factor

The cross-correlation depends on the scattering and fading conditions of the channel. Depending on the relation between the main component and the scattered components, the received signal by two antennas can have different cross-correlation levels. A known method of determining the scattering characteristics of the channel is by estimating the Ricean k-factor. Industrial environments are generally assumed to be Rayleigh channels due to the reflection from metallic structures. However, Chapter 2 describes a diverse number of industrial environments where this assumption cannot be valid in all cases. Thus, the Ricean k-factor can be used to identify the scattering levels in different industrial environments. Note that environments exhibiting a Ricean k-factor equal to zero correspond to Rayleigh fading channels.

Let us start defining the probability density function of a Ricean distribution

$$f_2(x) = \frac{x}{\hat{\sigma}^2} J_0\left(\frac{\hat{s}x}{\hat{\sigma}^2}\right) e^{-\frac{x^2+\hat{s}^2}{2\hat{\sigma}^2}}, \qquad x \geq 0 \tag{6.4}$$

where $J_0()$ is the Bessel function of zero-order and the parameters $\hat{\sigma}$ and $\hat{s}$ can be obtained from the received signal samples using several methods; namely, method of moments [76–78], method of maximum likelihood [79] and method of least squares [80]. In this case, we use the method of moments due to the lower computational time required for the estimation.

The estimation of the Ricean parameters using the method of moments is described as follows

$$\hat{\sigma} = \sqrt{\frac{E[x^2]}{2(\hat{k}+1)}} \tag{6.5}$$

$$\hat{s} = \sqrt{E[x^2] - \frac{E[x^2]}{\hat{k}+1}} \tag{6.6}$$

being $E[.]$ the expected value and $\hat{k}$

$$\hat{k} = \frac{\sqrt{1-\hat{\xi}}}{1-\sqrt{1-\hat{\xi}}} \tag{6.7}$$

and $\hat{\xi}$ is given by

$$\hat{\xi} = \frac{v[x^2]}{E[x^2]^2} \tag{6.8}$$

where $v[.]$ corresponds to the variance.

Diversity Techniques

Multiple techniques can be implemented to combine the received signals and increase the signal-to-noise ratio (SNR). Selection, feedback, equal gain and maximal ratio combining are some of the most extended combining techniques. In this thesis, selection combining (SC) and maximal ratio combining (MRC) are implemented [81]. The received signal-to-noise ratio after selection combining in two antenna system can be estimated as

$$\mathrm{SNR}_{SC}(n) = \frac{max\left\{x(n), y(n)\right\}}{\sqrt{B}}, \qquad n = 0, 1, \cdots, N-1 \tag{6.9}$$

where N is the length of the received signal and B is the noise power. In this case, we consider that both antennas are corrupted by uncorrelated white Gaussian noise with zero-mean and identical, B, noise power.

Applying maximal ratio combining diversity, the received signal-to-noise ratio after normalizing the power of each branch can be formulated by

$$\mathrm{SNR}_{MRC}(n) = \frac{\sqrt{x^2(n)+y^2(n)}}{\sqrt{B}}, \qquad n = 0, 1, \cdots, N-1 \tag{6.10}$$

The diversity gain obtained by using multiple antennas separated by a certain distance at a certain reliability level, p, can be computed as

$$G_{Div}(p) = \mathrm{SNR}_{Div}(p) - \mathrm{SNR}_{Ini}(p) \tag{6.11}$$

where $\mathrm{SNR}_{Div}(p)$ is the signal-to-noise ratio at p after combining signals and SNR_{Ini} is the signal-to-noise ratio without diversity.

6.3 Measurement Results and Analysis

The measurements presented in this chapter are product of a measurement campaign in two different industrial environments and an office corridor. The industrial environments

correspond to the bark furnace, i.e., the highly reflective environment, and a large storage hall similar to the metal works environment presented in Chapter 2. The office corridor is a typical office scenario as described also in Chapter 2.

The setup to study the spatial diversity in industrial environments is based on the spectrum analyzer setup presented in Chapter 2. The setup is composed of a signal generator connected to an antenna and two spectrum analyzers connected to two antennas [74]. The signal generator is transmitting a constant tone in the 433 MHz or 868 MHz ISM bands. A pulse generator is used to synchronize the spectrum analyzers and produce a common reference. The computer connected to both SAs defines the triggering time to start the measurements in the SAs and captures the data. The transferred data in the computer is used to compute the cross-correlation between receiving signals, Ricean k-factor and diversity gain when combining the signals.

In Figure 6.1, we can observe the cross-correlation between the two antennas at different distances for the three measured environments at 433 MHz. In this case, the cross-correlation values are the product of eight realizations for each antenna separation. Both industrial environments present lower cross-correlation levels than the corridor. The large storage hall has the lowest values, implying that the storage hall will present the greatest improvement when implementing spatial diversity. Additionally, we can observe that industrial environments have lower cross-correlation than the values given by Clarke's model (6.3), especially at short distances. This is due to Clarke's model does not take in account the mutual coupling between antennas as a consequence of placing them in the near field, and because they are receiving multi-path components from a broad angle of arrival.

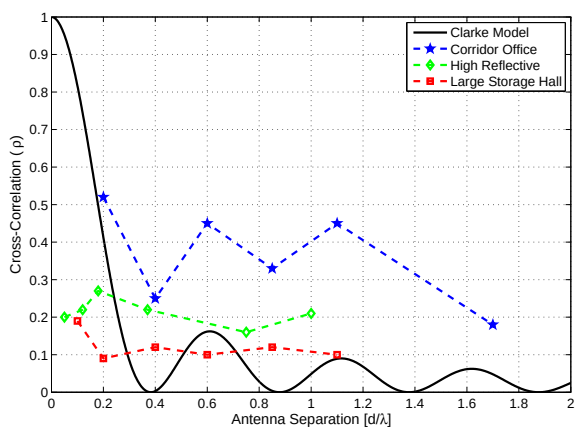

Figure 6.1: Average antenna cross-correlation versus antenna distance for 433 MHz (LoS) in different environments.

This spatial diversity study has also been performed at 868 MHz. The results of this study can be found in Paper [J5].

Combining the two received signals using selection combining and maximal ratio combining, the received SNR can be improved. For instance, Figure 6.2 shows the estimated CDF of the SNR for both antennas and the resulting SNR after combining them with selection combining and maximal ratio combining at 433 MHz for a cross-correlation value equal to 0.11. In this case, the diversity gain at 99% reliability is 9.62 dB for selection combining and 10.1 dB for maximal ratio combining.

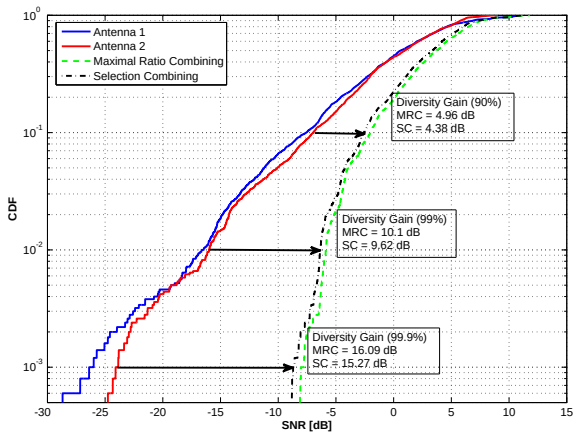

Figure 6.2: CDF of the received signals and the resulting combination, for 433 MHz (LoS) and $\lambda/8$ in the large storage hall.

Moreover, the Ricean k-factor of each environment is calculated according to (6.7). The k-factors in both industrial environments range from 0.16 to 1.32. These k-factor levels are close to zero, which is the k-factor in a Rayleigh environment. Table 6.1 contains the k-factors and the cross-correlation of the different environments for the 433 MHz frequency band at an antenna separation distance equal to $\lambda/5$. The table provides the average diversity gains by selection combining and maximal ratio combining. The diversity gain estimated in the large storage hall at 99% reliability is 10.79 dB for maximal ratio combining, and the diversity gain appears to be higher than that reported in previous indoor measurements [15].

Table 6.1: Estimated parameters for the different measured scenarios at 433 MHz with antenna separation of $\lambda/5$.

	K-factor	Cross-Corr.	Gain SC $[dB]$	Gain MRC $[dB]$
Corridor Office	0.24 - 1.36	0.39 - 0.64	4.26	5.14
High Reflective	0.16 - 0.55	0.11 - 0.67	9.03	9.52
Large Storage Hall	0.35 - 1.32	0.01 - 0.13	10.31	10.79

6.4 Discussion

This chapter investigated the potential benefits of using spatial diversity in wireless communication systems in industrial environments. As discussed in Chapter 3, industrial environments generally exhibit high multi-path levels. The multi-path can be used for improving the SNR of the wireless system by combining the signals from two spatially separated antennas. This improvement in the SNR is dependent on the antenna separation. Unfortunately, a number of industrial processes pose physical limitations to long spatial separations. In this work, the spatial diversity in an office corridor and two industrial environments with different characteristics is studied at 433 MHz. Thus, the cross-correlation, Ricean k-factor and the diversity gain from implementing selection combining and maximal ratio combining are estimated in the different environments.

The study of cross-correlation shows values lower than 0.35 in both industrial environments, even at short antenna separation distances, i.e., $\lambda/8$. The Ricean k-factor follows a trend similar to the cross-correlation, presenting low values in reflective environments. The benefits of using spatial diversity are greater than reported in previous studies, providing a diversity gain of up to 10.31 dB for selection combining and 10.79 dB for maximal ratio combining at $\lambda/5$. The measurement results show the possibility of setting short antenna separation in highly reflective industrial environments.

Chapter 7

Impulsive Noise Detection and Suppression

7.1 Introduction

Previous chapters presented a channel characterization of different industrial environments and studied the degradations found in such environments, namely multi-path, path loss and EMI. The objective of this chapter is to mitigate multi-path and EMI degradations. Orthogonal frequency-division multiplexing (OFDM) is an extended technique implemented in wireless systems that can cope with the multi-path degradation present in industrial environments. However, OFDM is sensitive to EMI of impulsive nature. This chapter studies the mitigation of EMI, improving the performance of wireless communication systems. By suppressing the source of interference, we can reduce the bit error rate (BER) and thus increase the reliability and robustness of the system. Figure 7.1 shows an example of the improved system performance when applying suppression techniques to the impulsive noise. The system can significantly reduce the BER, achieving levels close to a channel affected entirely by AWGN.

The suppression of interference depends on the ability to detect and separate the interference from the desired signal. In this manner, the mitigation of the impulsive noise is carried out in a two stage process, i.e., detection and suppression. Previous studies have investigated and developed efficient solutions for signal detection [16, 17, 82]. These techniques provide high probabilities of detection for different impulsive noise occurrences, i.e., impulsive rates. Unfortunately, the probability of occurrence of impulsive noise depends on the source of interference.

Regarding the suppression, multiple research studies have implemented non-linear techniques for suppressing impulsive noise, namely clipping, blanking or a combination of these two techniques [18, 19, 83]. Systems implementing these techniques experience significant reductions in interference degradation, although the reductions are strongly dependent on the threshold levels used when applying clipping and blanking to the interference. These thresholds are usually set to a fixed value; however, the strength of the signal

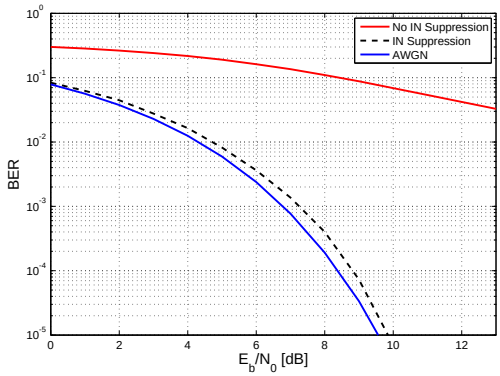

Figure 7.1: OFDM link performance under impulsive noise applying suppression.

and the impulsive noise amplitude can vary over time and between different scenarios. Moreover, the work performed in [20] investigates the suppression of the impulsive noise by using an OFDM pre-demodulated estimation of the signal. This technique in combination with the non-linear approaches mentioned earlier is studied in [84], suppressing the impulsive noise efficiently as shown in Figure 7.1.

OFDM is a technique with high levels of peak-to-average ratio (PAPR). Communication systems using OFDM need to implement PAPR reduction techniques to provide a signal with higher energy efficiency. The reduction of the PAPR can be used to set a more restrictive threshold, increasing the number of detected impulsive samples and thus, improving the performance of the system. Detection techniques implemented in OFDM systems do not provide good performance for OFDM-PAPR signals. This is due to different statistical properties of OFDM-PAPR signal compared to those of a purely OFDM signal [85]. Thus, a detection technique designed for OFDM systems, such as the Gaussian hypothesis described in [16], is not efficient for non-Gaussian distributed signals, i.e., OFDM-PAPR signals.

This chapter discusses multiple detection and suppression techniques to improve the robustness of the communication system against impulsive noise. The chapter is mainly structured in two parts. The first part investigates improvements in detection and suppression algorithms for OFDM systems, which are product of Paper [J6], while the second part studies detection techniques for non-Gaussian distributed signals such as OFDM-PAPR signals as presented in Paper [C5].

The content of this chapter is structured as follows. The next section presents the theoretical background of the detection and suppression techniques implemented in OFDM and OFDM-PAPR systems. The results of the detection and suppression performance analysis are presented in the third section. The last section of the chapter discusses the overall content of the chapter.

7.2 OFDM Systems in Environments with Impulsive Noise

This section contains the theoretical background of the different detection and suppression techniques implemented in the thesis.

The channel produces different degradations in the transmitted signal, namely, multi-path, path loss and impulsive interference, as we have shown in previous chapters. The received signal under these degradations can be expressed as

$$r(t) = \sum_{l=0}^{P-1} h_l s\left(t - \tau_l\right) + w(t) + i(t) \tag{7.1}$$

where h_l and τ_l are the complex-Gaussian channel coefficient and the delay of path l, respectively, $w(t)$ is the AWGN process, $i(t)$ is the impulsive noise defined in Chapter 5 as a composition of impulses with high amplitude in time domain and $s(t)$ is the transmitted signal. In this case, we use a robust technique to cope with the multi-path fading, i.e., OFDM, testing the effect of impulsive noise in the transmitted signal. The equivalent lowpass of the transmitted signal is formulated as

$$s_l(t) = \sum_{k=0}^{K-1} S_{n,k} e^{j2\pi \frac{k}{T_q} t}, \quad (n-1)T_q \leq t < n \cdot T_q \tag{7.2}$$

where K is the number of subcarriers, $S_{n,k}$ is the data symbol transmitted in subcarrier k during the nth symbol interval, $T_q = (T_G + T_u)$ is the symbol period being $1/T_u$ the frequency separation between two neighboring subcarriers, and T_G the guard time interval.

After sampling the received signal at the sample rate $1/T_s = M/T_u$ we obtain

$$\begin{aligned} r_{n,m} &= r(nT_u + mT_s), \quad m = 0, 1, \cdots, M-1 \\ &= \sum_{l=0}^{P-1} h_l s\left(nT_u + mT_s - \tau_l\right) + w_{n,m} + i_{n,m} \end{aligned} \tag{7.3}$$

where M is the oversampling rate, $w_{n,m}$ is the AWGN sample and $i_{n,m}$ is the impulsive noise sample.

Considering an OFDM system with a cyclic prefix longer that the maximum delay spread of the channel, the received signal sample at subcarrier k during the nth symbol interval can be written as follows

$$R_{n,k} = H_{n,k} S_{n,k} + W_{n,k} + I_{n,k}, \quad k = 0, 1, \cdots, K-1 \tag{7.4}$$

PAPR Reduction

OFDM signals have high PAPR levels. To increase the efficiency of the communication system a reduction of the PAPR needs to be applied. Many techniques have been proposed for reducing the PAPR in OFDM systems, such as coding [86], amplitude clipping [87], pulse shaping [88, 89], partial transmit sequence (PTS) [90] and selected mapping (SLM)

[91]. In papers [92, 93], comparison and overviews between the different techniques are presented. This thesis implements selected mapping for reducing the PAPR of OFDM systems presented in Paper [C5].

The OFDM signal described previously forms OFDM symbols following

$$X = [X_0, X_1, ..., X_{K-1}]^T \tag{7.5}$$

where $[.]^T$ denotes the transpose and K is the number of subcarriers of the OFDM symbol modulated with M-QAM.

The SLM technique creates a number of sequences, V, with uniformly distributed random phases between 0 and 2π [94]. These phase sequences are multiplied by the OFDM vector, (7.5), conforming a matrix with V different versions of the OFDM vector

$$\boldsymbol{X}^v = X\boldsymbol{\phi} = \begin{bmatrix} X_0\phi_{0,0} & \cdots & X_0\phi_{0,V-1} \\ X_1\phi_{1,0} & \cdots & X_1\phi_{1,V-1} \\ \vdots & \ddots & \vdots \\ X_{K-1}\phi_{K-1,0} & \cdots & X_{K-1}\phi_{K-1,V-1} \end{bmatrix} \tag{7.6}$$

This matrix contains V OFDM vectors having V PAPR. The PAPR of each version created by the SLM technique is calculated as

$$\mathrm{PAPR} = \frac{max\{\mid x^v(t) \mid^2\}}{E\{\mid x^v(t) \mid^2\}} \tag{7.7}$$

Thus, the version of the OFDM symbol with the minimum PAPR is subsequently selected for transmission

$$\tilde{X} = X\tilde{\phi} \tag{7.8}$$

The reduction of the PAPR when using the SLM technique was investigated by Bäuml [94]. This work defines the probability that the PAPR is higher than a certain level, PAPR_0, as

$$Pr\left\{\mathrm{PAPR} > \mathrm{PAPR}_0\right\} = \left(1 - \left(1 - e^{-\mathrm{PAPR}_0}\right)^K\right)^V \tag{7.9}$$

7.2.1 Impulsive Noise Detection

The identification of impulsive noise in the received signal is performed by using a combination of detecting techniques, as proposed in Paper [J6]. First, the Fisher's quadratic discriminator [95] is implemented to obtain part of the impulsive samples with a high impulsive rate. Second, the detected impulsive samples are blanked and finally, the Gaussian hypothesis estimation [16] is used to detect the impulsive samples with a lower impulsive rate. The combination of these detecting techniques, i.e., the Max detector, increases the probability of detection for a wide range of impulsive rates.

The block diagram of the combined detector is shown in Figure 7.2. The combination is constructed as follows: First, the received signal is inserted into Fisher's block, providing

a threshold Th_F. Second, the samples above this threshold, Th_F, are blanked resulting in a signal z with fewer impulses. Third, z is then inserted into the Gaussian hypothesis detector, giving a more accurate threshold Th_{FG}. Finally, by selecting the most restrictive threshold between Th_F and Th_{FG}, namely, Th_M, the technique computes the impulsive rate of the received signal.

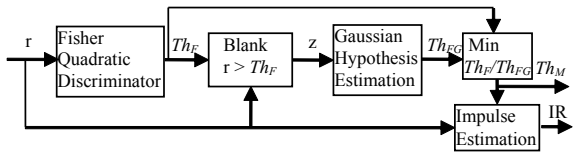

Figure 7.2: Block diagram of Max detector.

This Max detector can be improved by applying iterative techniques. By increasing this chain with another Gaussian hypothesis at the end of the Max detector, we can obtain higher probabilities of detection. This structure provides higher probability of detection, but consequently, the probability of false alarm begins to increase. We should note that an iterative detection structure improves the performance of the detector with the drawback of increasing the processing resource requirements.

Detection in OFDM-PAPR systems

The amplitude of the OFDM symbol follows a Gaussian process; however, implementing PAPR reduction techniques varies the amplitude distribution of the transmitted signal. The study reported in [96] investigated the envelope distribution of OFDM signals implementing SLM, defining the instant normalized sample power as

$$z_n = \frac{|r_n|^2}{E\left[|r|^2\right]} \quad n = 0, 1, \cdots, N-1 \tag{7.10}$$

being N the number of samples of the received blocked, r_n the discretized received signal and $E\left[|r|^2\right]$ the mean of r. Thus, the work in [96] defines the probability that the envelope exceeds a certain ratio level z_0

$$Pr\left\{z_n > z_0\right\} = 1 - \left(1 - \left(1 - \left(1 - e^{-z_0}\right)^K\right)^V\right)^{1/K} \tag{7.11}$$

where K and V are the number of subcarriers and SLM sequences respectively.

Based on this result, Paper [C5] proposes to estimate the detection threshold in OFDM systems using SLM. Selecting the desired probability, the normalized sample power, z_t, in (7.11) is obtained, and thus the detection threshold, Th_R, can be estimated from (7.10) as

$$Th_R = \sqrt{|z_t| E\left[|r|^2\right]} \tag{7.12}$$

7.2.2 Impulsive Noise Suppression

Multiple studies have investigated techniques for suppressing the impulsive noise in a received signal [18, 97]. This section contains techniques to suppress the impulsive noise

implemented in Papers [J6] and [C5]. The techniques implemented in these papers and described in this thesis are blanking, clipping-blanking non-linearity and suppression based on a pre-demodulated OFDM signal.

Non-linear Impulsive Suppression Technique

Clipping, blanking and clipping-blanking combination are among the non-linear techniques used to mitigate the impulsive noise. The following points describe blanking and clipping-blanking combination.

- Impulsive Noise Blanking

Blanking is an efficient technique used to suppress the impulsive noise [98]. This technique is commonly used in many studies due to its low implementation cost. Blanking impulsive noise samples consists of setting to zero the samples that are above a certain threshold

$$y_{n,m} = \begin{cases} r_{n,m} & |r_{n,m}| \leq Th_B \\ 0 & otherwise \end{cases} \tag{7.13}$$

where Th_B is the blanking threshold provided by the detection stage.

- Impulsive Noise Clipping-Blanking Combination

Previous studies have investigated the performance of clipping-blanking combination with respect to simply blanking or clipping the impulsive noise sample [97]. This study shows that combining clipping and blanking provides better performance than a single clipping or blanking. Clipping-blanking technique cuts or sets to zero the impulsive noise samples following the estimated thresholds. The signal after clipping-blanking can be defined as

$$y_{n,m} = \begin{cases} r_{n,m} & |r_{n,m}| < Th_C \\ Th_C \, e^{j \arg(r_{n,m})} & Th_C < |r_{n,m}| < Th_B \\ 0 & |r_{n,m}| > Th_B \end{cases} \tag{7.14}$$

where Th_C and Th_B are the estimated thresholds for clipping and blanking, respectively.

OFDM Pre-demodulated Suppression

A suppression technique that uses the pre-demodulated OFDM signal in combination with non-linear impulsive noise suppression techniques to improve the performance of an OFDM system is studied in [20] . This technique is applied after partially reducing the impulsive noise with a non-linear block. The signal after the non-linear block is pre-demodulated, subtracting additional impulsive samples before the final demodulation. In this section, we propose to use the previously described Max detector to improve the performance of the suppression technique. The block diagram of the entire impulsive noise suppression process is illustrated in Figure 7.3 and is divided into two steps. The first step corresponds to the non-linear impulsive noise suppression and the second to the OFDM pre-demodulated suppression. The algorithm for suppressing the impulsive noise of Step 2 can be found in Paper [J6].

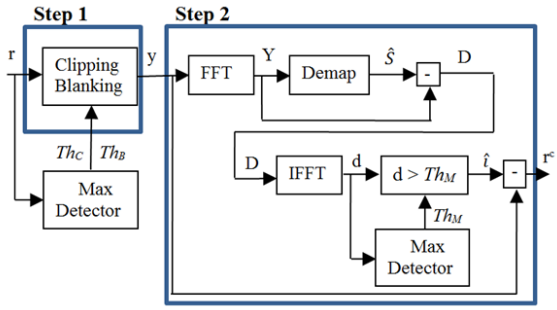

Figure 7.3: Block diagram of the impulsive noise suppression algorithm.

7.3 Measurement Results and Analysis

This section presents the simulation and measurement results of the detection and suppression techniques. The section is divided into two parts. The first part discusses the performance of the different detection and suppression techniques in OFDM systems product of Paper [J6]. The second part presents the performance of the detection techniques for an OFDM system using SLM technique to reduce the signal PAPR. The second part is based on the content of Paper [C5].

7.3.1 Detection and Suppression in OFDM Systems

Paper [J6] proposes an OFDM receiver structure for detecting and suppressing the impulsive noise. Figure 7.4 presents the proposed flow chart of the receiver. The receiver is composed of a detection and suppression blocks. The detection block corresponds to the Max detector described previously, and the suppression block corresponds to the combination of clipping-blanking and the OFDM pre-demodulated estimation. The OFDM receiver inserts the signal into the detection block and if the impulsive rate, IR, is higher than the desired level, β, the signal passes to the suppressing block. In the absence of impulsive noise, the signal is demodulated by a common OFDM receiver without expending resources in the suppressing block.

The objective of a detection block consists of estimating a threshold to distinguish signal samples from impulsive samples. To compare the performance of the different detectors, we define the optimum threshold as the threshold that provides the highest probability of detection for the minimum probability of false alarm. This corresponds to the maximum level of signal after passing through an AWGN channel

$$Th_O = max\{|s_{n,m} + w_{n,m}|\}, \quad n = 0, 1, \cdots, N-1 \tag{7.15}$$

being N the number samples.

The estimated thresholds from the different techniques are shown in Figure 7.5 (left) where the signal envelope and the impulsive noise are also shown. The Max detector and

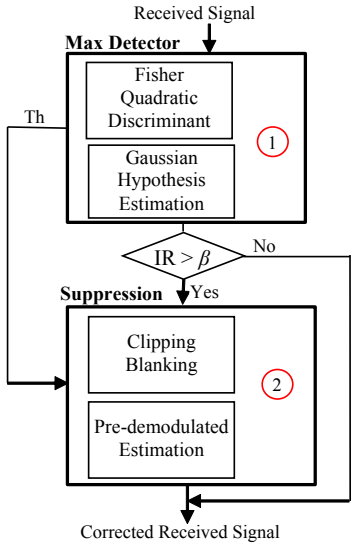

Figure 7.4: Flow chart diagram for the proposed receiver structure.

the iterative Max detector provide thresholds close to the optimum. Fisher's quadratic discriminator and Gaussian hypothesis estimate thresholds above the optimal and consequently misclassify impulsive samples. The performance of the detection techniques is illustrated in Figure 7.5 (right). The Gaussian hypothesis provides higher probability of detection than the Fisher's quadratic discriminator for impulses rates lower than 0.1. By combining the Fisher's quadratic discriminator and Gaussian hypothesis, i.e., the Max detector, an improved detector is obtained with equal or higher probability of detection compared to each of them separately. Observe in Figure 7.5 (right) for an impulsive rate equal to $IR = 0.3$, where the Max detector has 20% higher probability of detection than Fisher's quadratic discriminator and 55% higher than the Gaussian hypothesis estimation.

The OFDM receiving structure is evaluated in the laboratory environment described in Chapter 2. To evaluate the system performance, a test bed emulating a communication system with an interference source degrading the system is designed. The test bed is based on the spectrum analyzer setup presented in Chapter 2. The test bed contains two signal generators and a signal analyzer connected to a PC. The PC uploads the OFDM signal to one signal generator and the impulsive noise to the second signal generator. During reception, the signal analyzer captures the interfered signal and transfers it to the PC.

Figure 7.6 shows the measurement results of the combination of the detecting and suppressing techniques when impulsive noise is present in the environment. The statistical properties of the impulsive noise transmitted by the second signal generator are $\Gamma = 47.7$ and $IR = 3.17 \times 10^{-2}$. The BER decreases by more than two decades for energy per bit to noise ratio i.e., E_b/N_0, levels higher than 10 dB.

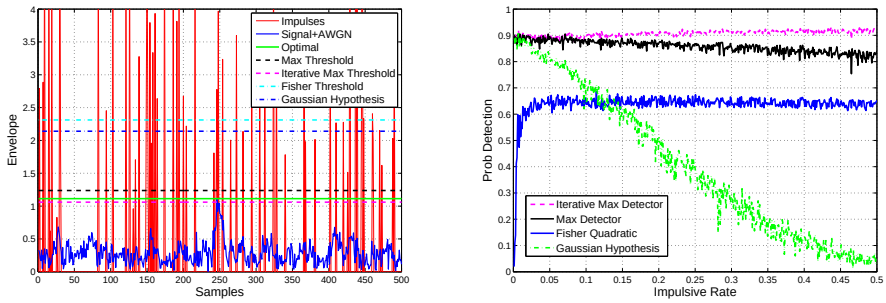

Figure 7.5: Signal, impulsive noise and thresholds performance at $IR = 0.1$ (left) and probability of detection versus impulsive rate for different detectors (right).

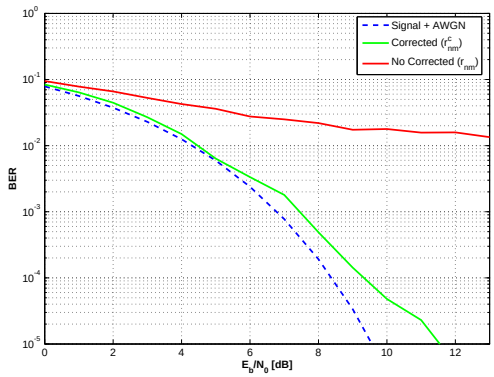

Figure 7.6: BER versus E_b/N_0 for measurements.

Furthermore, OFDM systems are often deployed in Rayleigh fading environments. Thus, this thesis studies the performance of an OFDM system interfered by an impulsive noise in a Rayleigh channel. To study the OFDM performance, an OFDM system interfered by impulsive noise with statistical properties equal to $\Gamma = 47.7$ and $IR = 3 \times 10^{-3}$, and with a Rayleigh channel composed of 10 complex-Gaussian taps, is simulated. Figure 7.7 (left) shows the performance of the system when the received signal is not corrected, $r_{n,m}$, when the signal is corrected after blanking non-linearity, $y_{n,m}$, and when applying the OFDM pre-demodulated suppression, $r^c_{n,m}$. The performance of the BER of the corrected signal, $r^c_{n,m}$, improves by more than two decades at $E_b/N_0 > 30$ dB with respect to the not corrected signal.

The degradation caused by the Rayleigh channel can be mitigated by applying diversity techniques to the system. Frequency diversity is a technique for reducing multi-path fading in frequency selective channels [99]. By transmitting a single data symbol in L OFDM

subcarriers, the probability that the data symbol suffers an amplitude depth fade in the L subcarriers is reduced. However, implementing frequency diversity reduces the transmission rate by the diversity factor used, $1/L$. In this thesis, a frequency diversity with $L = 2$ is used for this study. The simulated results of the OFDM system when frequency diversity is implemented are illustrated in Figure 7.7 (right). The overall OFDM receiver with frequency diversity can mitigate the impulsive noise reaching BER lower than 5×10^{-6} in a Rayleigh channel.

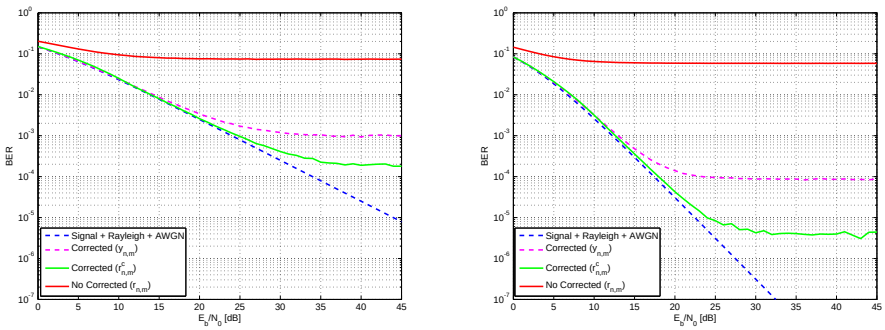

Figure 7.7: Simulated BER versus E_b/N_0 in a Rayleigh channel (left) and with frequency diversity, $L = 2$, (right).

7.3.2 Detection and Suppression in OFDM-PAPR Systems

This part describes the performance of detection techniques for an OFDM signal when PAPR reduction by SLM is applied. Reducing the PAPR changes the amplitude distribution of the OFDM signal. A proposed detection technique is used to estimate the suppressing threshold and improve the performance of the system. Paper [C5] contains the results of the proposed detection technique for OFDM-SLM systems.

The performance of the detection techniques is evaluated for impulsive noise with different statistical properties. For this purpose, the impulsive rate, IR, and the impulsive amplitude, Γ are swept over a wide range of values. First, the amplitude of the impulses is fixed to $\Gamma = 10$, and the probability of detection is estimated at different IR, as shown in Figure 7.8 (left). The probability of detection increases by more than 30% in the impulsive rate range between 10^{-3} and 0.1. Second, the probability of detection is studied with respect to the impulsive amplitude, Γ, for an impulsive rate fixed to $IR = 10^{-2}$. The probability of detection increases to 38% higher than the Gaussian hypothesis estimation at $IR = 10^{-2}$; the results of this study can be found in Paper [C5]. The probability of false alarm maintains values lower than 10^{-6} for all the different cases.

The detected impulses are blanked (7.13); therefore, the corrected signal after detection and suppression results in an improved performance of the system. In Figure 7.8 (right), we can observe the BER of the system for different values of IR. The overall system

shows an improvement in the BER with respect to the Gaussian hypothesis of more than one decade and up to four decades with respect to the signal before impulsive detection and suppression.

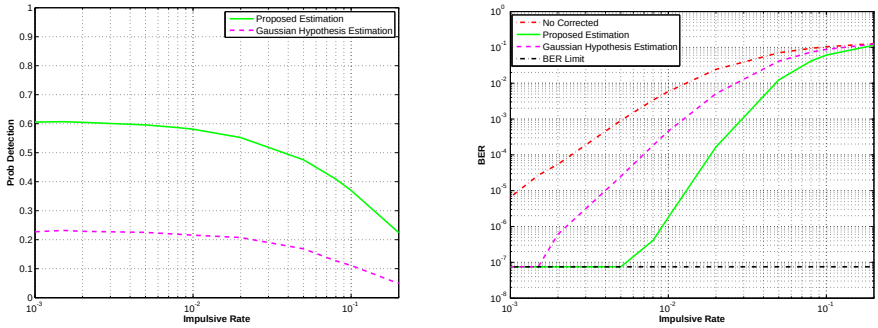

Figure 7.8: Probability of detection (left) and BER (right) with respect to IR for the proposed detection and Gaussian hypothesis estimation at $\Gamma = 10$.

7.4 Discussion

This chapter studied impulsive noise detection and suppression techniques. The chapter investigates a combination of detection techniques to provide an efficient detector to address impulsive noise with a wide range of statistical properties. The impulsive samples detected are suppressed in two steps: clipping-blanking and OFDM pre-demodulated estimation. This chapter proposes a receiving structure, combining detection and suppression stages, providing an improvement in the BER of the system. This improvement is evaluated through simulations and measurements in a laboratory test bed. The results show a substantial improvement in the BER for AWGN and Rayleigh channels.

Furthermore, detection techniques for non-Gaussian signals, such as OFDM-PAPR, are also investigated. This chapter proposed a detection technique that exploits the statistical properties of the amplitude distribution in an OFDM-PAPR signal. Thus, impulsive noise samples with low amplitudes are distinguished, thereby improving the detection probability and the overall performance of the OFDM system.

Chapter 8

Conclusions

8.1 Concluding Remarks

The deployment of wireless communications in industrial environments has grown rapidly in recent years, and this trend is expected to continue. The low cost and scalability of wireless systems provide excellent benefits for the industrial sector. However, part of the industrial sector refuses to deploy wireless solutions, questioning the reliability of these solutions. Multiple sources of degradation can arise, reducing the performance of the communication system and its reliability. This thesis analyzed a wide range of industrial environments, characterizing the sources of degradation and suggesting improvements to combat the degradations that these environments introduce into wireless systems.

Industrial environments are generally classified as environments with large dimensions containing multiple metallic objects and high levels of EMI. This general description of industrial environments is valid for a large percentage of environments. However, certain industrial environments exhibit different structural characteristics, behaving on some occasions in an opposite manner. A characterization of diverse industrial environments is necessary to identify the sources of degradation and increase the reliability of the wireless systems.

Chapter 2 presented a broad variety of industrial environments with different propagation characteristics. These industrial environments were characterized in Chapters 3 through 5, identifying the main sources of degradation. To characterize the channel, different measurements setups have been developed, estimating the time dispersion, path loss and EMI characteristics of the environments. Chapter 3 discussed the time dispersion of the environments, distinguishing between industrial environments with high and low delay spreads. Low delay spread industrial environments have not been identified in the literature review. This finding increases the understanding of special industrial environments and provides valuable information for system developers. Chapter 4 presented a path loss characterization in different industrial environments. This characterization finds a stronger frequency dependence of the path loss in NLoS scenarios than that reported in previous works. In Chapter 5, a number of EMI sources captured in industry are reported. The

characterized EMI observed in our study present higher frequency components than those reported in the literature. This study can be used to investigate the effect of EMI on the performance of wireless systems.

The characterization of the diverse industrial environments presented in Chapter 2 results in an environment classification in terms of the different degradation levels found in these environments. This concluding chapter provides an overview of the characterized industrial environments based on an extended measurement campaign presented in Chapters 3 through 5. Figure 8.1 illustrates the industrial environments classification in terms of EMI and multi-path levels estimated in the different environments.

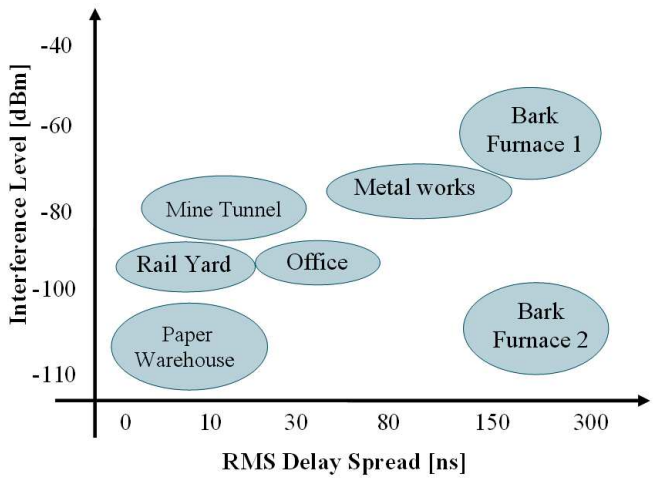

Figure 8.1: Industrial environment classification in terms of interference and multi-path levels.

The overall environment classification can be divided into two groups; environments with higher and lower rms delay spreads relative to a reference office environment. The first group contains bark furnaces 1 and 2, and metal works. Bark furnaces 1 and 2 correspond to industrial environments with similar dimensions and structural characteristics. The dense presence of metallic objects in both of these environments produces high time dispersion and rms delay spread levels. However, bark furnace 1 exhibits higher interference levels than bark furnace 2 due to the presence of larger quantities of electrical machinery. The metal works can be considered as the typical industrial environment with large dimensions and presence of metallic objects. This environment produces high delay spread levels that are lower than the previous bark furnace environments. In the metal works, interference degradation can also be a problem as result of the presence of the transportation vehicles and electrical motors.

The second group with a lower rms delay spread relative to the office environment contains mine tunnels, rail yards and paper warehouses. Mine tunnels are special environments

with low rms delay spread levels due to the particular characteristics of the tunnel structure. Trains loading and releasing raw material can produce EMI over a wide frequency band. Rail yards are outdoor environments with large dimensions and a large number of trains and electric pantographs. These elements are sources of EMI for the wireless communications. The paper warehouse has larger dimensions than bark furnaces 1 and 2, containing piled rolls of paper. These paper rolls absorb the signals, mitigating the strength of possible EMI. However, at the same time, the paper rolls absorb the multi-path components, producing a radio coverage problem in NLoS situations due to the significant path loss fading levels. This radio coverage problem eliminates the possibility of using systems that take advantage of multi-path propagation effects. A path loss characterization in the paper warehouse shows a strong frequency dependence that could be related to the dielectric properties of the paper. To provide a reference environment, an office environment was characterized and illustrated among this industrial environment classification. Office environments exhibit multi-path and interference levels that correspond to typical indoor environments, such as houses and buildings.

By charactering the different sources of degradation in industrial environments, we acquire additional knowledge on how to design and select wireless technologies with the greatest reliability and robustness. Furthermore, increasing the knowledge of the degradation sources in an industrial environment can decrease the risk of incidents, where personnel and material can be harmed.

Following the industrial environment characterization, this thesis studied spatial diversity and impulsive noise mitigation techniques for improving the performance of industrial wireless systems.

Spatial diversity is often used to reduce the multi-path fading characteristics of a channel. Significant gain can be achieved by using multiple antennas at the transmitter/receiver sites when separating the antennas by a certain distance. Unfortunately, some industrial processes present physical restrictions that make large antenna separations impossible. In Chapter 6, we presented measurements characterizing the cross-correlation, Ricean k-factor and diversity gain with respect to the antenna separation distance. Environments with significant time dispersion can potentially be used for implementing spatial diversity techniques. Chapter 6 shows that industrial environments with high delay spread properties can set a separation distance shorter than $\lambda/5$. At such distances, the wireless systems can achieve diversity gains up to 10.79 dB, increasing the reliability of the communication system.

Regarding the impulsive noise mitigation, multiple techniques for detecting and suppressing impulsive noise have been reported in previous works. However, existing impulsive noise detectors performance is highly dependent on the statistical properties of the transmitted signal and impulsive noise. This thesis proposes an OFDM receiving structure that combines detection and suppression techniques for mitigating impulsive noise with different statistical properties. The receiving structure is tested in AWGN and multi-path fading channels, showing an important improvement in the performance of the system. Furthermore, the thesis also presents detection techniques in scenarios where the transmitted signal is non-Gaussian distributed, i.e., OFDM-PAPR.

The overall contribution of this thesis can be summarized as follows. This thesis is

a novel work, characterizing industrial environments with diverse structural properties by identifying the main sources of degradation in each environment. The thesis is novel work investigating the benefits of applying spatial diversity at short antenna separations in high delay spread industrial environments. The thesis is a novel work studying high performance impulsive noise detection and suppression techniques in OFDM systems under impulsive noise with different statistical properties. The results of this thesis could be used by the industrial sector to implement safer and more reliable wireless solutions in a diverse variety of industrial environments.

8.2 Future Directions

This section discusses possible directions for future work. This thesis characterized the propagation characteristics in diverse industrial environments at different frequency bands. However, the development of wireless systems at frequencies higher than 3 GHz produces a need for characterizing the analyzed industrial environments at a wider frequency range. Moreover, the time for performing the measurements campaigns in some industrial environments was restricted due to the ongoing industrial activities. It might therefore be interesting to perform new measurement campaigns at higher frequency bands and using greater number of measurement points and positions in the analyzed environments.

As the last section reported, the particular properties of the studied industrial environments provide different sources of degradation to the wireless system. It might be interesting to extend the characterization of the channel by performing measurements in environments with different characteristics and sources of degradations. A potential direction for continuing the work performed in this thesis could be to characterize other environments, such as nuclear plants, electricity substations, hospitals, storage halls such as those in Ikea and subway tunnels. These environments require high reliability levels in their communications and have special properties that can degrade the wireless performance.

This thesis characterized and modeled multi-path propagation in different industrial environments. However, it might be interesting to formulate a multi-path model that can predict the statistical impulsive response of the channel. This model could be dependent on the structural dimensions of the building, elements present in the environments and the dielectric properties of the building and elements. A prediction of the multi-path behavior could therefore direct the selection of a reliable wireless system for a specific environment.

In Chapter 4, the path loss characterization of the paper warehouse showed a strong frequency dependence at certain frequency bands. A deeper study of the dielectric properties of the paper might be an interesting continuation for clarifying this frequency dependence in NLoS scenarios.

The performance of a detection technique is dependent on the statistical properties of the signal. Thus, another topic of certain interest might be the study of the performance of the detection and suppression techniques proposed in this thesis on other types of signals, such as spread spectrum signals, for instance, in code division multiple access (CDMA).

Bibliography

[1] Ericsson AB, "Ericsson mobility report - on the pulse of the networked society," White Paper, Nov. 2013.

[2] Cisco, "Cisco visual networking index: Global mobile data traffic forecast update, 2013 - 2018," White Paper, Feb. 2014.

[3] R. Thusu, "Wireless sensor use is expanding in industrial applications," Frost & Sullivan Sensors, Jun. 2010.

[4] R. Primerano, K. Wanuga, J. Dorn, M. Kam, and K. Dandekar, "Echo-cancellation for ultrasonic data transmission through a metal channel," in *Annual Conference on Information Sciences and Systems*, 2007, pp. 841–845.

[5] K. A. Remley, G. Koepke, C. Grosvenor, R. Johnk, J. Ladbury, D. Camell, and J. Coder, "NIST tests of the wireless environment in automobile manufacturing facilities," *Natl. Inst. Stand. Technol. Note 1550*, Oct. 2008.

[6] X. Wang, Y. Ren, J. Zhao, Z. Guo, and R. Yao, "Comparison of ieee 802.11e and ieee 802.15.3 mac," in *Proceedings of the IEEE 6th Circuits and Systems Symposium on Emerging Technologies: Frontiers of Mobile and Wireless Communication*, vol. 2, May 2004, pp. 675 – 680.

[7] P. Radmand, A. Talevski, S. Petersen, and S. Carlsen, "Comparison of industrial wsn standards," in *IEEE International Conference on Digital Ecosystems and Technologies*, Apr. 2010, pp. 632 –637.

[8] J. Karedal, S. Wyne, P. Almers, F. Tufvesson, and A. Molisch, "UWB channel measurements in an industrial environment," in *IEEE Global Telecommunications Conference*, vol. 6, Nov. 2004, pp. 3511 – 3516.

[9] S. Kjesbu and T. Brunsvik, "Radiowave propagation in industrial environments," in *IEEE Annual Conference of Industrial Electronics Society (IECON)*, vol. 4, 2000, pp. 2425–2430.

[10] E. Tanghe, W. Joseph, L. Verloock, L. Martens, H. Capoen, K. Van Herwegen, and W. Vantomme, "The industrial indoor channel: large-scale and temporal fading at

900, 2400, and 5200 mhz," *IEEE Trans. on Wireless Communications*, vol. 7, no. 7, pp. 2740–2751, 2008.

[11] H. A. Myers, "Industrial equipment spectrum signatures," *IEEE Trans. on Radio Frequency Interference*, vol. 5, no. 1, pp. 30–42, 1963.

[12] E. N. Skomal, "Comparative radio noise levels of transmission lines, automotive traffic, and rf stabilized arc welders," *IEEE Trans. on Electromagnetic Compatibility*, vol. 9, no. 2, pp. 73–77, 1967.

[13] S. Diggavi, "On achievable performance of spatial diversity fading channels," *IEEE Trans. on Information Theory*, vol. 47, no. 1, pp. 308 –325, Jan 2001.

[14] P. Shamain and L. Milstein, "Detection with spatial diversity using noisy channel estimates in a correlated fading channel," in *Proceedings MILCOM*, vol. 1, Oct. 2002, pp. 691 – 696.

[15] J. Dietrich, C.B., K. Dietze, J. Nealy, and W. Stutzman, "Spatial, polarization, and pattern diversity for wireless handheld terminals," *IEEE Trans. on Antennas and Propagation*, vol. 49, no. 9, pp. 1271–1281, 2001.

[16] P. Torio and M. G. Sanchez, "Improving capability of detecting impulsive noise," *IEEE Trans. on Electromagnetic Compatibility*, vol. PP, no. 99, pp. 1 –8, Jul. 2012.

[17] T. Oliveira, P. Correia de Sa and, S. de Paula Barbosa, M. Ribeiro, and C. Marques, "Hos-based impulsive noise detection technique for power line communication systems," in *IEEE International Symposium on Power Line Communications and Its Applications*, Mar. 2010, pp. 125 –130.

[18] T. Hirakawa, M. Fujii, M. Itami, and K. Itoh, "A study on iterative impulse noise reduction in ofdm signal by recovering time domain samples," in *IEEE International Symposium on Power Line Communications and Its Applications*, 2006, pp. 325 – 330.

[19] R. Fantacci, A. Tani, and D. Tarchi, "Impulse noise mitigation techniques for xdsl systems in a real environment," *IEEE Trans. on Consumer Electronics*, vol. 56, no. 4, pp. 2106 –2114, Nov. 2010.

[20] S. Zhidkov, "Impulsive noise suppression in ofdm-based communication systems," *IEEE Trans. on Consumer Electronics*, vol. 49, no. 4, pp. 944 – 948, Nov. 2003.

[21] J. Karedal, S. Wyne, P. Almers, F. Tufvesson, and A. Molisch, "A measurement-based statistical model for industrial ultra-wideband channels," *IEEE Trans. on Wireless Communications*, vol. 6, no. 8, pp. 3028–3037, Aug. 2007.

[22] O. Staub, J.-F. Zurcher, P. Morel, and A. Croisier, "Indoor propagation and electromagnetic pollution in an industrial plant," in *International Conference on Industrial Electronics, Control and Instrumentation*, vol. 3, 1997, pp. 1198–1203.

[23] E. Tanghe, W. Joseph, L. Martens, H. Capoen, K. Van Herwegen, and W. Vantomme, "Large-scale fading in industrial environments at wireless communication frequencies," in *Antennas and Propagation Society International Symposium*, 2007, pp. 3001–3004.

[24] T. S. Rappaport, "Wireless communications: Principles and practice," 2008.

[25] J. Kivinen, X. Zhao, and P. Vainikainen, "Empirical characterization of wideband indoor radio channel at 5.3 ghz," *IEEE Trans. on Antennas and Propagation*, vol. 49, no. 8, pp. 1192–1203, 2001.

[26] S. Ghassemzadeh, L. Greenstein, T. Sveinsson, A. Kavcic, and V. Tarokh, "Uwb delay profile models for residential and commercial indoor environments," *IEEE Trans. on Vehicular Technology*, vol. 54, no. 4, pp. 1235–1244, 2005.

[27] R. He, Z. Zhong, B. Ai, K. Guan, B. Chen, J. Aionso, and C. Briso, "Propagation channel measurements and analysis at 2.4 ghz in subway tunnels," *IET Microwaves, Antennas Propagation*, vol. 7, no. 11, pp. 934–941, 2013.

[28] C. Nerguizian, C. Despins, S. Affes, and M. Djadel, "Radio-channel characterization of an underground mine at 2.4 ghz," *IEEE Trans. on Wireless Communications*, vol. 4, no. 5, pp. 2441–2453, 2005.

[29] I. Mabrouk, L. Talbi, M. Nedil, Y. Coulibaly, and T. Denidni, "Effect of antenna directivity on performance of multiple input multiple output systems in an underground gold mine," *IET Microwaves, Antennas Propagation*, vol. 6, no. 5, pp. 555–561, 2012.

[30] M. Varela and M. Sanchez, "RMS delay and coherence bandwidth measurements in indoor radio channels in the UHF band," *IEEE Trans. on Vehicular Technology*, vol. 50, no. 2, pp. 515 –525, Mar. 2001.

[31] H. Anderson and J. McGeehan, "Direct calculation of coherence bandwidth in urban microcells using a ray-tracing propagation model," in *IEEE International Symposium on Personal, Indoor and Mobile Radio Communications*, vol. 1, Sep. 1994, pp. 20–24.

[32] M. Sanchez, A. Hammoudeh, E. Grindrod, and J. Kermoal, "Coherence bandwidth characterization in an urban microcell at 62.4 ghz," *IEEE Trans. on Vehicular Technology*, vol. 49, no. 2, pp. 607–613, Mar. 2000.

[33] A. A. M. Saleh and R. Valenzuela, "A statistical model for indoor multipath propagation," *IEEE Journal on Selected Areas in Communications*, vol. 5, no. 2, pp. 128–137, Feb. 1987.

[34] C. Holloway, M. Cotton, and P. McKenna, "A model for predicting the power delay profile characteristics inside a room," *IEEE Trans. on Vehicular Technolog*, vol. 48, no. 4, pp. 1110–1120, Jul. 1999.

[35] T. Rappaport, "Indoor radio communications for factories of the future," *IEEE Communications Magazine*, vol. 27, no. 5, pp. 15–24, 1989.

[36] H. Al-Tamimi and S. Al-Qaraawy, "Uwb propagation indoor statistical channel modeling," in *International Colloquium on Computing, Communication, Control, and Management*, vol. 1, 2009, pp. 379–383.

[37] Y. Okumura, E. Ohmori, T. Kawano, and K. Fukuda, "Field strength and its variability in vhf and uhf land-mobile radio service," *Rev. Elec. Com. Lab.*, vol. 16, pp. 825–873, 1968.

[38] M. Hatay, "Empirical formula for propagation loss in land mobile radio services," *IEEE Trans. on Vehicular Technology*, vol. 29, no. 3, pp. 317–325, 1980.

[39] C. A. (231), "Digital mobile radio towards future generation systems, final report," *Tec. report, European Communities, EUR 18957*, 1999.

[40] M. Chamchoy, W. Doungdeun, and S. Promwong, "Measurement and modeling of uwb path loss for single-band and multi-band propagation channel," in *IEEE International Symposium on Communications and Information Technology*, vol. 2, 2005, pp. 991–995.

[41] N. Blaunstein and Y. Ben-Shimol, "Prediction of frequency dependence of path loss and link-budget design for various terrestrial communication links," *IEEE Trans. on Antennas and Propagation*, vol. 52, no. 10, pp. 2719–2729, 2004.

[42] D. Chizhik, "Clutter height variation and its effect on frequency dependence of radio path loss," in *Proceedings of the 5th European Conference on Antennas and Propagation (EUCAP)*, 2011, pp. 3444–3447.

[43] S. Geng and P. Vainikainen, "Experimental investigation of the properties of multiband uwb propagation channels," in *IEEE 18th International Symposium on Personal, Indoor and Mobile Radio Communications*, 2007, pp. 1–5.

[44] A. F. Molish, K. Balakrishnan, D. Cassioli, C. C. Chong, A. F. S. Emami, J. Karedal, J. Kunisch, H. Shantz, U. Shuster, and K. Siwiak, "IEEE 802.15.4a channel model - final report," 2005.

[45] A. Molisch, "Ultrawideband propagation channels-theory, measurement, and modeling," *IEEE Trans. on Vehicular Technology*, vol. 54, no. 5, pp. 1528–1545, 2005.

[46] M. Sanchez, I. Cuinas, and A. Alejos, "Interference and impairments in radio communication systems due to industrial shot noise," in *IEEE International Symposium on Industrial Electronics*, 2007, pp. 1849–1854.

[47] J. Catrysse and K. Vantomme, "Characterization of the EM noise inside machines related to wireless communication systems," Paris, Jun. 2007.

[48] F. Zare, "Practical approach to model electric motors for electromagnetic interference and shaft voltage analysis," *IET Electric Power Applications*, vol. 4, no. 9, pp. 727–738, 2010.

[49] A. Wefky, F. Espinosa, and et al., "Modeling radiated electromagnetic emissions of electric motorcycles in terms of driving profile using mlp neural networks," *Progress In Electromagnetics Research, University of Alcala*, vol. 135, pp. 231–244, 2013.

[50] R. Rizzi, A. Orlandi, G. Antonini, and V. Ricchiuti, "Electromagnetic interferences on implantable medical devices onboard of high speed trains," in *IEEE International Symposium on Electromagnetic Compatibility*, vol. 3, 2006, pp. 674–679.

[51] A. Morant, A. Wisten, D. Galar, U. Kumar, and S. Niska, "Railway emi impact on train operation and environment," in *International Symposium on Electromagnetic Compatibility (EMC EUROPE)*, 2012, pp. 1–7.

[52] R. Shepherd, "Measurements of amplitude probability distributions and power of automobile ignition noise at HF," *IEEE Trans. on Vehicular Technology*, vol. 23, no. 3, pp. 72 – 83, Aug. 1974.

[53] K. Wiklundh, "An approach to using amplitude probability distribution for emission limits to protect digital radio receivers using error-correction codes," *IEEE Trans. on Electromagnetic Compatibility*, vol. 52, no. 1, pp. 223 –229, Feb. 2010.

[54] J. Wang, T. Tayamachi, and O. Fujiwara, "Amplitude probability distribution measurement for electric field intensity assessment of cellular-phone-base stations," *IEEE Trans. on Electromagnetic Compatibility*, vol. 50, no. 3, pp. 736 –739, Aug. 2008.

[55] Y. Yamanaka and T. Shinozuka, "Measurement and estimation of BER degradation of PHS due to electromagnetic disturbances from microwave ovens," pp. 55 – 63, Nov. 1998.

[56] H. Kanemoto, S. Miyamoto, and N. Morinaga, "A study on modeling of microwave oven interference and optimum reception," in *IEEE International Symposium on Electromagnetic Compatibility*, vol. 1, Aug. 1998, pp. 57 –62.

[57] K. Gotoh, Y. Matsumoto, S. Ishigami, T. Shinozuka, and M. Uchino, "Development and Evaluation of a Prototype Multichannel APD Measuring Receiver," in *IEEE International Symposium on Electromagnetic Compatibility*, Jul. 2007, pp. 1 –6.

[58] H. H. Slim, C. Hoffmann, S. Braun, and P. Russer, "A novel multichannel amplitude probability distribution for a time-domain EMI measurement system according to CISPR 16-1-1," in *EMC Europe 2011 York*, Sep. 2011, pp. 22 –25.

[59] D. Middleton, "Man-made noise in urban environments and transportation systems: Models and measurements," *IEEE Trans. on Communications*, vol. 21, no. 11, pp. 1232–1241, Nov. 1973.

[60] ——, "Statistical-physical models of electromagnetic interference," *IEEE Trans. on Electromagnetic Compatibility*, vol. EMC-19, no. 3, pp. 106–127, Aug. 1977.

[61] S. Zabin and H. Poor, "Parameter estimation for middleton class a interference processes," *IEEE Trans. on Communications*, vol. 37, no. 10, pp. 1042–1051, Oct. 1989.

[62] P. Torio and M. Sanchez, "Mitigation of impulsive noise in digital video broadcasting terrestrial using orthogonal polarization reception," *IEEE Trans. on Consumer Electronics*, vol. 55, no. 4, pp. 1798–1804, 2009.

[63] Y. Ma, P. So, E. Gunawan, and Y. Guan, "Analysis of impulsive noise and multipath effects on broadband power line communications," in *International Conference on Power System Technology*, vol. 2, Nov. 2004, pp. 1404–1409.

[64] Y. Neuvo and W. Ku, "Analysis and digital realization of a pseudorandom gaussian and impulsive noise source," *IEEE Transactions on Communications*, vol. 23, no. 9, pp. 849 – 858, Sep. 1975.

[65] CISPR 16-2-3 (2nd Ed), "Specification for radio disturbance and immunity measuring apparatus and methods - part 2-3: Methods of measurement of disturbances and immunity - radiated disturbance measurements," Mar. 2006.

[66] M. Sanchez, L. de Haro, M. Ramon, A. Mansilla, C. Ortega, and D. Oliver, "Impulsive noise measurements and characterization in a uhf digital tv channel," *IEEE Trans. on Electromagnetic Compatibility*, vol. 41, no. 2, pp. 124–136, 1999.

[67] H. Mecke, R. Doebbelin, and T. Wlnkler, "Cost-effective mitigation measures concerning conducted emission of resistance welding inverters," in *International Symposium on Electromagnetic Compatibility and Electromagnetic Ecology*, 2005, pp. 25–29.

[68] T. Winkler, R. Doebbelin, and A. Lindemann, "Mitigation of conducted emission of power electronic resistance welding equipment," in *Power Electronics and Motion Control Conference*, 2006, pp. 450–455.

[69] W. C. Y. Lee, "Antenna spacing requirement for a mobile radio base-station diversity," *Bell System Technical Journal*, vol.50, pp. 1859-1876, Jul. 1971.

[70] Y. Jiang, K. Li, J. Gao, and H. Harada, "Antenna space diversity and polarization mismatch in wideband 60ghz-millimeter-wave wireless system," in *IEEE 20th International Symposium on Personal, Indoor and Mobile Radio Communications*, 2009, pp. 1781–1785.

[71] J. Lempiainen and J. Laiho-Steffens, "The performance of polarization diversity schemes at a base station in small/micro cells at 1800 mhz," *IEEE Trans. on Vehicular Technology*, vol. 47, no. 3, pp. 1087–1092, 1998.

[72] B.-K. Kim, W. Stutzman, and D. Sweeney, "Indoor and outdoor measurements of space, polarization, and angle diversity for cellular base stations in urban environments," in *IEEE Vehicular Technology Conference 52nd*, vol. 1, 2000, pp. 22–29.

[73] A. M. d. Turkmani, A. Arowojolu, P. A. Jefford, and C. J. Kellett, "An experimental evaluation of the performance of two-branch space and polarization diversity schemes at 1800 mhz," *IEEE Trans. on Vehicular Technology*, vol. 44, no. 2, pp. 318–326, 1995.

[74] J. Colburn, Y. Rahmat-samii, M. Jensen, and G. Pottie, "Evaluation of personal communications dual-antenna handset diversity performance," *IEEE Trans. on Vehicular Technology*, vol. 47, no. 3, pp. 737–746, 1998.

[75] R. H. Clarke, "A statistical theory of mobile-radio reception," *Bell System Technical Journal* 47:6, pp. 957-1000, Aug., 1968.

[76] A. Abdi, C. Tepedelenlioglu, M. Kaveh, and G. Giannakis, "On the estimation of the k parameter for the rice fading distribution," *IEEE Communications Letters*, vol. 5, no. 3, pp. 92–94, Mar.

[77] C. Tepedelenlioglu, A. Abdi, G. Giannakis, and M. Kaveh, "Performance analysis of moment-based estimators for the k parameter of the rice fading distribution," in *IEEE International Conference on Acoustics, Speech, and Signal Processing*, vol. 4, 2001, pp. 2521–2524.

[78] L. Greenstein, D. Michelson, and V. Erceg, "Moment-method estimation of the ricean k-factor," *IEEE Communications Letters*, vol. 3, no. 6, pp. 175–176, 1999.

[79] J. Sijbers, A. den Dekker, P. Scheunders, and D. Van Dyck, "Maximum-likelihood estimation of rician distribution parameters," *IEEE Trans. on Medical Imaging*, vol. 17, no. 3, pp. 357–361, Jun. 1998.

[80] Z. Mei, Z. Chenghui, Z. Huanshui, C. Peng, and D. Yanchun, "Robust least square method and its application to parameter estimation," in *IEEE International Conference on Automation and Logistics*, Aug. 2007, pp. 1483–1486.

[81] W. C. Jakes, "Microwave mobile communications," *IEEE Press, New York* 1993.

[82] A. Muqaibel, B. Woerner, and S. Riad, "Application of multiuser detection techniques to impulse radio time hopping multiple access systems," in *IEEE Conference onUltra Wideband Systems and Technologies*, 2002, pp. 169 – 173.

[83] T. Kitamura, K. Ohno, and M. Itami, "Improving of performance of ofdm reception under class-a impulsive channel by replica signal estimation of impulse," in *IEEE International Conference on Consumer Electronics (ICCE)*, Jan. 2012, pp. 620 –621.

[84] K. Al-Mawali, A. Sadik, and Z. Hussain, "Joint time-domain/frequency-domain impulsive noise reduction in ofdm-based power line communications," in *Telecommunication Networks and Applications Conference*, Dec. 2008, pp. 138 –142.

[85] H. Ochiai and H. Imai, "On the distribution of the peak-to-average power ratio in ofdm signals," *IEEE Trans. on Communications*, vol. 49, no. 2, pp. 282–289, Feb. 2001.

[86] S. Slimane, "Reducing the peak-to-average power ratio of ofdm signals through precoding," *IEEE Trans. on Vehicular Technology*, vol. 56, no. 2, pp. 686–695, 2007.

[87] R. O'Neill and null, "Envelope variations and spectral splatter in clipped multicarrier signals," in *IEEE International Symposium on Personal, Indoor and Mobile Radio Communications. Wireless: Merging onto the Information Superhighway*, vol. 1, 1995, pp. 71–75.

[88] Y. Jian, Z. Zang, and W.-Y. Yan, "Papr distribution analysis of ofdm signals with pulse shaping," in *Asia-Pacific Conference on Communications*, Oct. 2005, pp. 473–477.

[89] S. Slimane, "Peak-to-average power ratio reduction of ofdm signals using broadband pulse shaping," in *Proceedings of Vehicular Technology Conference*, vol. 2, 2002, pp. 889–893.

[90] L. Yang, R. Chen, Y. Siu, and K. Soo, "Papr reduction of an ofdm signal by use of pts with low computational complexity," *IEEE Trans. on Broadcasting*, vol. 52, no. 1, pp. 83–86, 2006.

[91] S.-J. Heo, H.-S. Noh, J.-S. No, and D.-J. Shin, "A modified slm scheme with low complexity for papr reduction of ofdm systems," *IEEE Trans. on Broadcasting*, vol. 53, no. 4, pp. 804–808, 2007.

[92] S. H. Han and J. H. Lee, "An overview of peak-to-average power ratio reduction techniques for multicarrier transmission," *IEEE Trans. on Wireless Communications*, vol. 12, no. 2, pp. 56 – 65, Apr. 2005.

[93] T. Jiang and Y. Wu, "An overview: Peak-to-average power ratio reduction techniques for ofdm signals," *IEEE Trans. on Broadcasting*, vol. 54, no. 2, pp. 257 –268, Jun. 2008.

[94] R. Bauml, R. Fischer, and J. Huber, "Reducing the peak-to-average power ratio of multicarrier modulation by selected mapping," *Electronics Letters*, vol. 32, no. 22, pp. 2056 –2057, Oct. 1996.

[95] K. Barbe and and W. Van Moer, "Automatic detection, estimation, and validation of harmonic components in measured power spectra: All-in-one approach," *IEEE Trans. on Instrumentation and Measurement*, vol. 60, no. 3, pp. 1061 –1069, Mar. 2011.

[96] K. Bae and E. Powers, "Distribution of envelope power using selected mapping in ofdm systems with nonlinearity," in *IEEE International Conference on Acoustics, Speech and Signal Processing*, 2008, pp. 3065–3068.

[97] S. Zhidkov, "Analysis and comparison of several simple impulsive noise mitigation schemes for ofdm receivers," *IEEE Trans. on Communications*, vol. 56, no. 1, pp. 5 –9, Jan. 2008.

[98] ——, "Performance analysis and optimization of ofdm receiver with blanking nonlinearity in impulsive noise environment," *IEEE Trans. on Vehicular Technology*, vol. 55, no. 1, pp. 234–242, 2006.

[99] P. Dirner and S. Lin, "Measured frequency diversity improvement for digital radio," *IEEE Trans. on Communications*, vol. 33, no. 1, pp. 106–109, Jan. 1985.

PAPER REPRINTS